Chapter 2

Semiconductor Laser Optical Phase-Locked Loops

2.1 OPLL Basics

The SCL-OPLL, shown in figure 2.1, is a feedback system that enables electronic control of the phase of the output of an SCL. The fields of the master laser and the slave SCL are mixed in a photodetector PD. A part of the detected photocurrent is monitored using an electronic spectrum analyzer. The detected output is amplified, mixed down with an "offset" radio frequency (RF) signal, filtered and fed back to the SCL to complete the loop.

A schematic model of the OPLL is shown in figure 2.2(a). We will assume that the free-running SCL has an output $a_s \cos\left(\omega_s^{fr} t + \phi_s^{fr}(t)\right)$, where the "phase noise" $\phi_s^{fr}(t)$ is assumed to have zero mean. When the loop is in lock, we drop the superscript fr from the laser phase and frequency variables. Similarly, the master laser output is given by $a_m \cos\left(\omega_m t + \phi_m(t)\right)$. The detected photocurrent is then

$$i_{PD}(t) = \rho\left(a_m^2 + a_s^2 + 2a_s a_m \cos\left[\left(\omega_m - \omega_s\right)t + \left(\phi_m(t) - \phi_s(t)\right)\right]\right), \qquad (2.1)$$

where ρ is the responsivity of the PD. The last term above shows that the PD acts as a frequency mixer in the OPLL. Let us further define a photodetector gain $K_{PD} \doteq 2\rho\left\langle a_s a_m \right\rangle$, where $\langle . \rangle$ denotes the average value. The detected photocurrent is then mixed down with a radio frequency (RF) signal, whose output is taken to

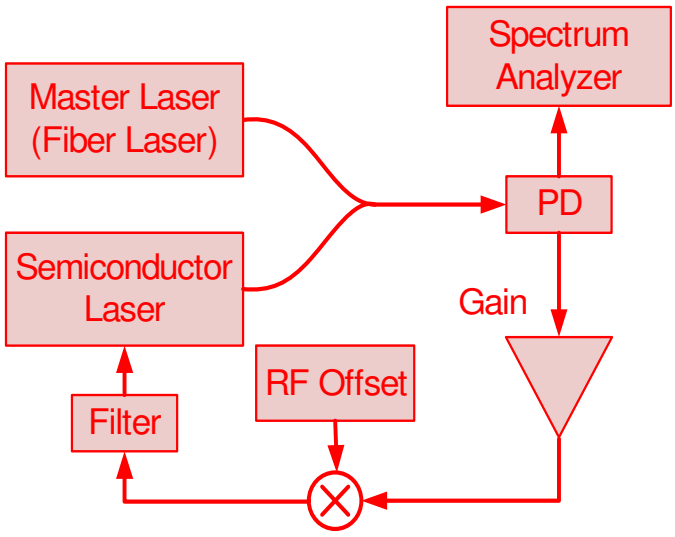

Figure 2.1. A heterodyne semiconductor laser optical phase-locked loop. PD: photo-detector.

be $a_{RF}\sin\left(\omega_{RF}t+\phi_{RF}(t)\right)$. The choice of trigonometric functions ensures a mixer output of the form

$$i_M(t)=\pm K_M K_{PD} a_{RF}\sin\left[\left(\omega_m-\omega_s\pm\omega_{RF}\right)t+\left(\phi_m(t)-\phi_s(t)\pm\phi_{RF}(t)\right)\right]. \qquad (2.2)$$

Without loss of generality, we will consider only the "+" sign in the rest of this thesis. This mixer output is amplified with gain K_{amp}, filtered and fed into the SCL, which acts as a current-controlled oscillator whose frequency shift is proportional to the input current, i.e.,

$$\delta\omega_s=-K_s i_s(t)=-K_s K_{amp} i_M(t) \qquad (2.3)$$

The minus sign indicates that the frequency of the SCL decreases with increasing current. A propagation delay τ_L is included in the analysis. We will assume that the filter has a unity gain at DC, i.e., the area under its impulse response is zero. We lump together the DC gains of the various elements in the loop, and denote it by K_{dc}, i.e., $K_{dc}=a_{RF}K_M K_{PD}K_{amp}K_s$. This parameter will shortly be defined in a more rigorous manner. When in lock, the frequency shift of the SCL is given by

$$\delta\omega_s=-K_{dc}\sin\left[\left(\omega_m-\omega_s\pm\omega_{RF}\right)t+\left(\phi_m(t)-\phi_s(t)\pm\phi_{RF}(t)\right)\right]. \qquad (2.4)$$

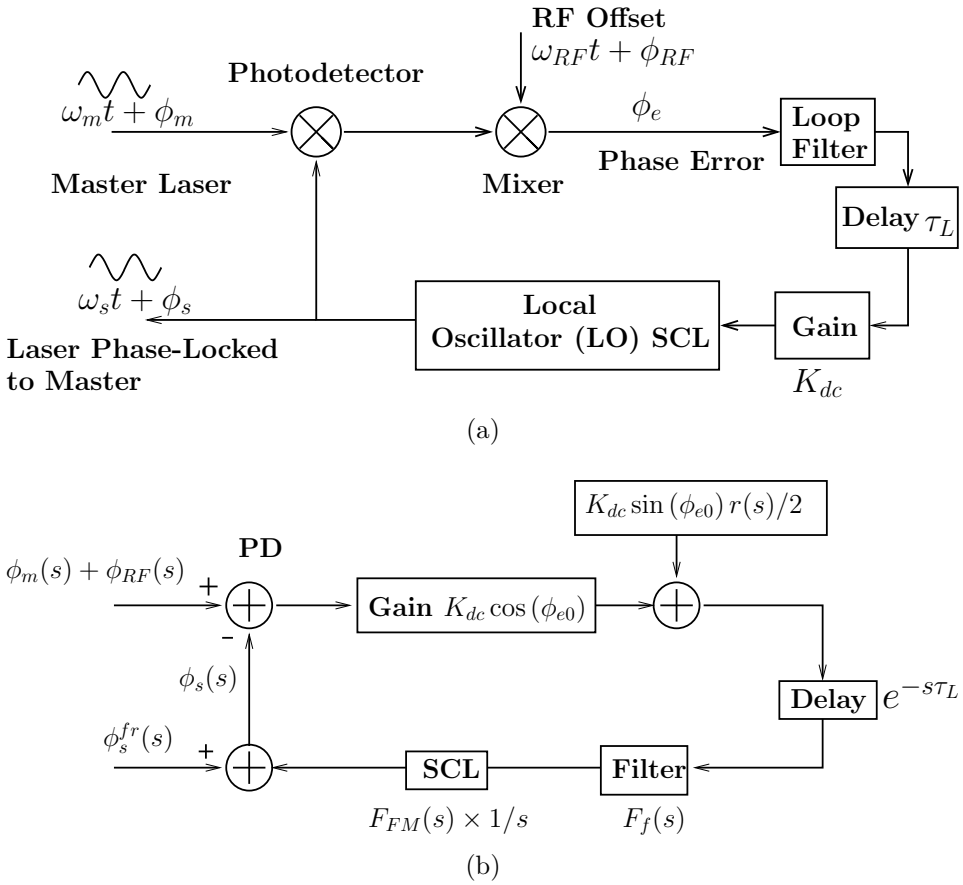

Figure 2.2. (a) Schematic diagram of an OPLL. (b) Linearized small-signal model for phase noise propagation in the OPLL.

The frequency of the slave laser is the sum of the free-running frequency and the correction from the feedback loop, i.e.,

$$\omega_s = \omega_s^{fr} + \delta\omega_s. \tag{2.5}$$

The free-running frequency difference between the slave and master lasers (offset by the RF frequency) is defined as

$$\Delta\omega_{fr} \doteq \omega_m - \omega_s^{fr} + \omega_{RF}. \tag{2.6}$$

We now derive the the steady-state operating point of this laser [2]. In steady state, the error signal at the output of the mixer (equation (2.2)) does not change with

time, which yields

$$\begin{aligned} \omega_s &= \omega_m + \omega_{RF}, \\ \bar{\phi}_s &= \bar{\phi}_m + \bar{\phi}_{RF} + \phi_{e0}. \end{aligned} \tag{2.7}$$

The bars in the second part of equation (2.7) denote that this equation is valid for the steady-state values of the phase. The parameter ϕ_{e0} is the steady-state phase error in the loop. This phase error is a consequence of the feedback current keeping the loop in lock, which can be understood by substituting equation (2.7) into equation (2.4) and using equations (2.5) and (2.6) to obtain

$$\delta\omega_s = \Delta\omega_{fr} = K_{dc} \sin \phi_{e0}. \tag{2.8}$$

The frequency shift induced by the feedback loop, $\delta\omega_s$, compensates for the free-running frequency difference between the slave and master lasers, and its maximum value is limited by the DC gain of the loop. The maximum value of the free-running frequency difference that the loop can tolerate in lock is called the "hold-in range," and is defined in section 2.1.2. The steady-state phase error is given by

$$\phi_{e0} = \sin^{-1}\left(\frac{\Delta\omega_{fr}}{K_{dc}}\right). \tag{2.9}$$

It is important that the DC gain K_{dc} be as large as possible and the laser free-running frequency fluctuations be minimized, so that ϕ_{e0} is small. Indeed, this is the case in most well-designed OPLLs, and we will ignore this steady state phase error in large parts of this thesis. In the absence of ϕ_{e0}, the phase of the locked slave SCL exactly follows that of the master laser, offset by the RF phase.

The heterodyne OPLL of figure 2.1 differs from the homodyne PLL shown in figure 1.1 in the addition of an extra reference ("offset") RF oscillator. This results in some powerful advantages: as is clear from equation (2.7), *the optical phase can be controlled in a degree for degree manner by adjusting the electronic phase of the offset signal.* Further, heterodyne locking ensures that the beat note at the photodetector is at an intermediate frequency, where it is away from low-frequency noise sources

and can easily be separated from the low frequency ("DC") terms.

2.1.1 Small-Signal Analysis

The OPLL is next linearized about the steady-state operating point given in equation (2.7) and the propagation of the phase around the loop is analyzed in the Laplace domain [2], as shown in figure 2.2(b). The variables in the loop are the Laplace transforms of the phases of the lasers and the RF signal.[1] Fourier transforms are also useful to understand some loop properties, and will be used in parts of the thesis. The Fourier transform $X(f)$ is the Laplace transform $X(s)$ evaluated along the imaginary axis, $s = j2\pi f$. The notation $X(\omega)$ is also used in literature to denote the Fourier transform, with the angular Fourier frequency, ω, given by $\omega = 2\pi f$; we will use $X(f)$ in this thesis to avoid confusion. It is to be understood that the steady-state values of the phase in equation (2.7) are subtracted from the phases before the Laplace (or Fourier) transform is computed. The free-running phase fluctuation of the slave SCL ("phase noise") is denoted by the additive term $\phi_s^{fr}(s)$.[2] The summed relative intensity noises of the lasers $r(s)$ are also incorporated into the model.[3]

The SCL acts as a current-controlled oscillator and, in the ideal case, produces an output phase equal to the integral of the input current for all modulation frequencies, i.e. it has a transfer function $1/s$. However, the response of a practical SCL is not ideal, and the change in output optical frequency is a function of the frequency components of the input current modulation. This dependence is modeled by a frequency-dependent FM response $F_{FM}(s)$. The shape of the FM response and

[1] Notation: the Laplace transform of the variable $x(t)$ is denoted by $X(s)$. For Greek letters, the Fourier transform of $\phi(t)$ is just denoted by $\phi(s)$. The argument s is sometimes dropped when the usage is clear from the context.

[2] Strictly speaking, the Laplace or Fourier transform of the phase noise cannot be defined—it is a random process, and we can only describe its spectral density. However, the use of Laplace transforms provides valuable insight—for this purpose, we can regard the observed phase noise as a particular instance of the underlying random process. The spectral density will be used in all calculations involving the phase noise, e.g., see chapter 3.

[3] The model of figure 2.2(b) is easily derived by noting that the expansion of the phase detector output $K_{dc}\,(1 + r(t)/2)\sin(\phi_{e0} + \phi_e(t))$ about the steady state value $K_{dc}\sin\phi_{e0}$ is $K_{dc}\sin\phi_{e0}$ + $(K_{dc}\sin\phi_{e0})\,r(t)/2$ + $(K_{dc}\cos\phi_{e0})\,\phi_e(t)$. The relative amplitude noise is one-half the relative intensity noise.

its effects are discussed in section 2.3. The filter response and the FM response of the SCL are assumed to be normalized to have unit gain at DC, i.e., $F_f(0) = 1$,[4] $F_{FM}(0) = 1$. For simplicity, we have also assumed that the photodetector and mixer have flat frequency responses—this is true if wideband detectors and mixers are used in the loop, as is the case in this work. It is straightforward to include nonuniform detector and mixer responses in the analysis.

Let us define the open-loop transfer function of the loop as the product of the transfer functions of all the elements in the loop for the ideal case $\phi_{e0} = 0$:

$$G_{op}(s) = \frac{K_{dc} F_f(s) F_{FM}(s) e^{-s\tau_L}}{s}. \tag{2.10}$$

This allows us to define the DC gain in a more rigorous manner:

$$K_{dc} \doteq \lim_{s \to 0} s G_{op}(s). \tag{2.11}$$

The phase of the locked SCL is then given by

$$\phi_s(s) = (\phi_m(s) + \phi_{RF}(s)) \frac{G_{op} \cos \phi_{e0}}{1 + G_{op} \cos \phi_{e0}} + \frac{\phi_s^{fr}(s)}{1 + G_{op} \cos \phi_{e0}} + \frac{r(s)}{2} \frac{G_{op} \sin \phi_{e0}}{1 + G_{op} \cos \phi_{e0}}, \tag{2.12}$$

where we have omitted the argument s in $G_{op}(s)$. Phase noise, $\phi_s^{fr}(s)$, represents the largest source of noise in an SCL-OPLL due to the relatively large linewidth of an SCL, and the contribution of the last term on the right-hand side can usually be neglected, especially if $\phi_{e0} \approx 0$. We will therefore ignore the laser relative intensity noise in the rest of this thesis. For similar reasons, we also neglect the effects of shot noise and detector noise on the phase of the SCL in this thesis. It will also be assumed, unless stated otherwise, that $\phi_{e0} = 0$.

[4]For some filter transfer functions, e.g., integrators, this normalization is not feasible. In such cases, we simply let $K_{dc} \to \infty$.

2.1.2 OPLL Performance Metrics

We now define the important OPLL performance metrics that will be used in this work.

Loop bandwidth is the largest Fourier frequency for which the open loop transfer function $G_{op}(f)$ is larger than unity. From equation (2.12), this means that *the phase of the locked SCL follows that of the master and the RF offset within the loop bandwidth, and reverts to the free-running value at higher frequencies.* The loop bandwidth is usually limited by the stability of the loop—in particular, we will use the Bode stability criterion [2], which states that the magnitude of the complex valued function $G_{op}(f)$ should be lesser than unity when its phase is lesser than or equal to $-\pi$. The frequency at which the phase response equals $-\pi$ is referred to as the "phase-crossover frequency" and represents the maximum possible value of the loop bandwidth.

Hold-in range is defined as the largest change in the free-running frequency of the slave SCL over which the loop still remains in lock. This can be evaluated from equation (2.8), where the sine function takes a maximum value of unity. Using equation (2.11), we write the hold-in range as

$$f_{hold} = \frac{1}{2\pi} \lim_{s \to 0} s G_{op}(s). \tag{2.13}$$

Clearly, a large hold-in range is desired so that the loop is insensitive to environmental fluctuations.

Residual phase error in the loop is one of the most important metrics to evaluate the performance of the loop. It is defined as the variance in the deviation of the phase of the locked SCL from the ideal case where it follows the master laser, i.e.,

$$\sigma_\phi^2 = \left\langle \left(\phi_s(t) - \phi_m(t) - \phi_{RF}(t)\right)^2 \right\rangle, \tag{2.14}$$

where $\langle . \rangle$ denotes averaging over all time.[5] Using the Wiener-Khintchine theorem, equation (2.14) can be written in the frequency domain as

$$\sigma_\phi^2 = \int_{-\infty}^{\infty} S_\phi^e(f)\, df, \tag{2.15}$$

where $S_\phi^e(f)$ is the spectral density of the random variable $\phi_s(t) - \phi_m(t) - \phi_{RF}(t)$, i.e., the spectrum of the phase error. Using equation (2.12), and assuming $\phi_{e0} = 0$, we have

$$S_\phi^e(f) = \left| \frac{1}{1 + G_{op}(f)} \right|^2 \left(S_\phi^m(f) + S_\phi^{s,fr}(f) \right), \tag{2.16}$$

where we have used the fact that the phase noise of the master laser and free-running slave laser are uncorrelated. $S_\phi^m(f)$ and $S_\phi^{s,fr}(f)$ are the spectra of the phase noise of the master and free-running slave SCL respectively, and the phase noise of the RF source is assumed to be negligible. Under the assumption of a Lorenzian lineshape for the lasers, these spectral densities are related to their 3 dB linewidths $\Delta\nu$ by [72]

$$\begin{aligned} S_\phi^m(f) &= \frac{\Delta\nu_m}{2\pi f^2}, \\ S_\phi^{s,fr}(f) &= \frac{\Delta\nu_s}{2\pi f^2}. \end{aligned} \tag{2.17}$$

Using (2.16) and (2.17) in (2.15), we obtain the result for the variance of the residual phase error of the OPLL:

$$\sigma_\phi^2 = \frac{\Delta\nu_m + \Delta\nu_s}{2\pi} \int_{-\infty}^{\infty} \frac{1}{f^2} \left| \frac{1}{1 + G_{op}(f)} \right|^2 df. \tag{2.18}$$

For a stable OPLL, we require that $\sigma_\phi^2 \ll 1$ rad^2. σ_ϕ is the standard deviation of the residual phase error, measured in radians.

Settling time is defined as the time taken by the error signal in the loop to relax back to its steady-state value, within 1%, when a step phase input $\Delta\phi$ is applied.

[5] For simplicity, we make the common assumption that the phase noise is a stationary process.

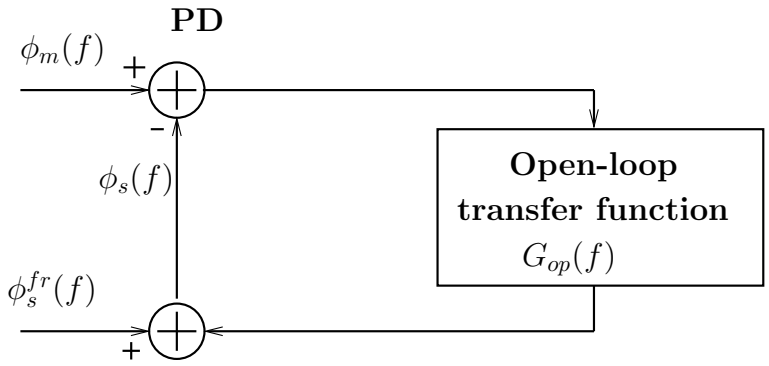

Figure 2.3. Simplified schematic diagram of an OPLL.

If the step is applied at $t = 0$, the phase error goes from $(\phi_{e0} + \Delta\phi)$ to $(\phi_{e0} + 0.01\Delta\phi)$ at time $t = \tau_s$. Alternatively, this is the time taken by the laser phase to change by $0.99\Delta\phi$. The settling time is of interest in applications where the laser phase is changed using an RF phase input.

The response of the loop error signal to a step input is given by

$$\phi_e(t) - \phi_{e0} = \mathcal{L}^{-1}\left[\Delta\phi \frac{1}{s\,(1 + G_{op}(s))}\right], \tag{2.19}$$

where $\mathcal{L}^{-1}$ is the inverse Laplace transform operator.

Other OPLL metrics such as acquisition range, mean time between cycle-slips etc. are not central to this work and will not be considered here. Some of these metrics are discussed in references [2, 73].

2.2 Performance of Different OPLL Architectures

We now evaluate the performance metrics listed above for three different OPLL architectures that are relevant to this work. In this section, we assume that the FM response of the SCL is flat, i.e., $F_{FM}(f) = 1$. The "type" of an OPLL is the number of poles[6] at $s = 0$, and its "order" is the total number of poles. The RF source is assumed to have no noise, which allows the OPLL to be simplified as in figure 2.3.

[6]A pole is a root of the equation $D(s) = 0$, where $D(s)$ is the denominator of the open-loop transfer function $G_{op}(s)$.

As a concrete example, let us assume that the summed linewidth of the master and slave lasers is 0.5 MHz, which is representative of (good) DFB SCLs.

2.2.1 Type I OPLL

This OPLL has a transfer function

$$G_{op}(f) = \frac{K}{j2\pi f}, \tag{2.20}$$

where the pole at $f = 0$ denotes that the optical phase at the output of the SCL is obtained by integrating the input control signal. The magnitude and phase of $G_{op}(f)$ are plotted in a "Bode plot" in figure 2.4(a). Since the phase of $G_{op}(f)$ never goes to $-\pi$, this OPLL is unconditionally stable, with bandwidth and hold-in range $K/2\pi$. Practical OPLLs are always bandwidth-limited; let us therefore arbitrarily assume that the bandwidth of this loop is 2 MHz, i.e., $K = 1.26 \times 10^7$ rad/s.

The laser frequency drifts due to fluctuations in the laser bias current and temperature. Assuming that a low noise current source is used to bias the laser, the primary source of *free-running* frequency variations is environmental temperature fluctuations. The thermal frequency tuning coefficient of InP-based lasers is typically 10 GHz/°C. A hold-in range of 2 MHz therefore means that the loop loses lock if the SCL temperature fluctuates by only $\sim 2 \times 10^{-4}$ °C.

The residual phase error of this loop is given by

$$\sigma_\phi^2 = \frac{\pi(\Delta\nu_m + \Delta\nu_s)}{K}, \tag{2.21}$$

which, with the assumed values of laser linewidth and loop bandwidth, yields $\sigma_\phi^2 = 0.4$ rad^2. Equation (2.21) leads us to an important general result: *it is necessary that the summed linewidths of the two lasers be much smaller than the loop bandwidth for good OPLL performance.*

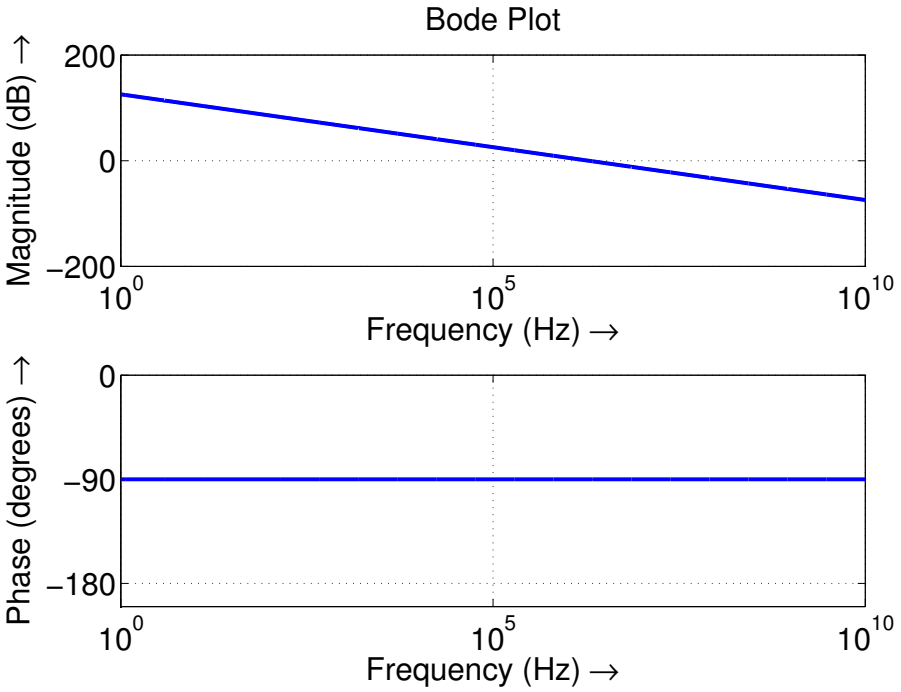

(a)

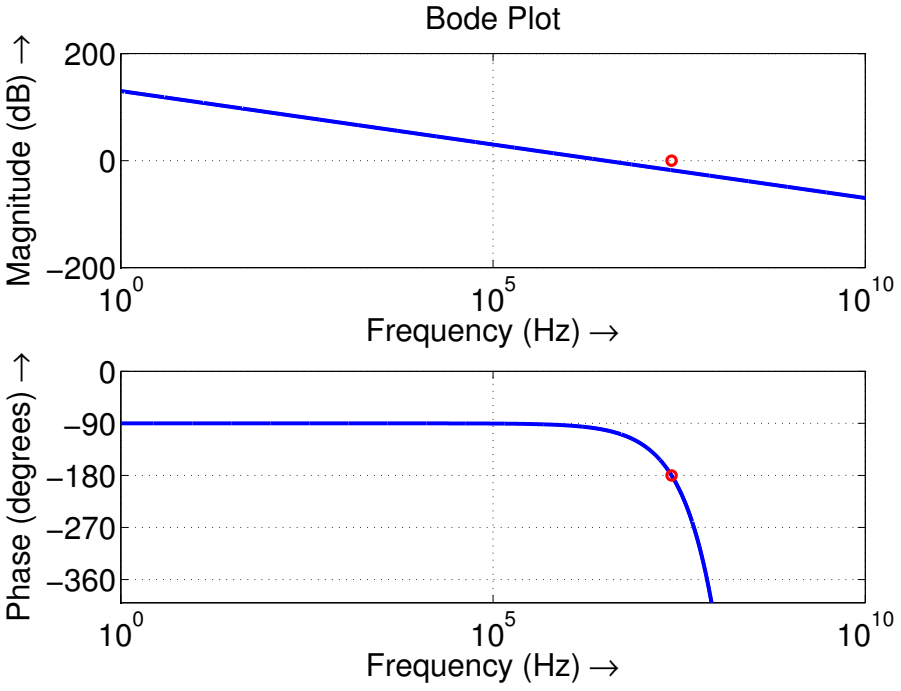

(b)

Figure 2.4. Bode plots for (a) a Type I OPLL and (b) a Type I OPLL with a propagation delay of 10 ns. The phase-crossover frequency is indicated by the marker in (b).

The response of the phase error to a step response is

$$\phi_e(t) - \phi_{e0} = \Delta\phi \exp(-Kt), \tag{2.22}$$

which gives a 99% settling time of $\tau_s \simeq 4.6/K \simeq 4 \times 10^{-7}$ s.

The high sensitivity of this loop to temperature fluctuations is due to the arbitrary bandwidth limit assumed; however other factors such as the SCL FM response and loop propagation delay, discussed later, do impose such a restriction. It is therefore important to design loop filters to increase the DC gain and loop bandwidth.

2.2.2 Type I, Second-Order OPLL

The extremely high sensitivity of the basic Type I OPLL to temperature fluctuations can be overcome using a filter $F_f(f) = (1 + j2\pi f\tau_0)/(1 + j2\pi f\tau_1)$, with $\tau_0 < \tau_1$. This filter is called a lag filter or lag compensator [74][7] since its response has a phase lag (phase response is <0). The value of τ_0 is chosen so that τ_0^{-1} is much smaller than the loop bandwidth, which ensures that the filter response does not affect the phase-crossover frequency. To maintain the same value of the loop bandwidth as the Type I OPLL, the loop gain has to be increased by a factor τ_1/τ_0, so that the loop transfer function is

$$G_{op}(f) = \frac{K}{j2\pi f} \times \frac{\tau_1}{\tau_0} \times \frac{1 + j2\pi f\tau_0}{1 + j2\pi f\tau_1}. \tag{2.23}$$

In the limit of $\tau_1 \to \infty$, this loop is a Type-II control system.

The bandwidth of this loop is $K/2\pi = 2$ MHz, while the hold-in range is $K\tau_1/2\pi\tau_0$. By proper choice of τ_1 and τ_0, a hold-in range of several gigahertz can be achieved. A hold-in range of 1 GHz corresponds to a temperature change of 0.1 °C, and the SCL temperature is easily controlled to much smaller than this value.

The addition of the lag filter at low frequencies does not affect the residual phase error σ_ϕ^2, since most of the contribution to the integral in equation (2.18) is from frequencies of the order of the loop bandwidth.

[7] Some authors, e.g., [2], refer to this filter as a lag-lead filter.

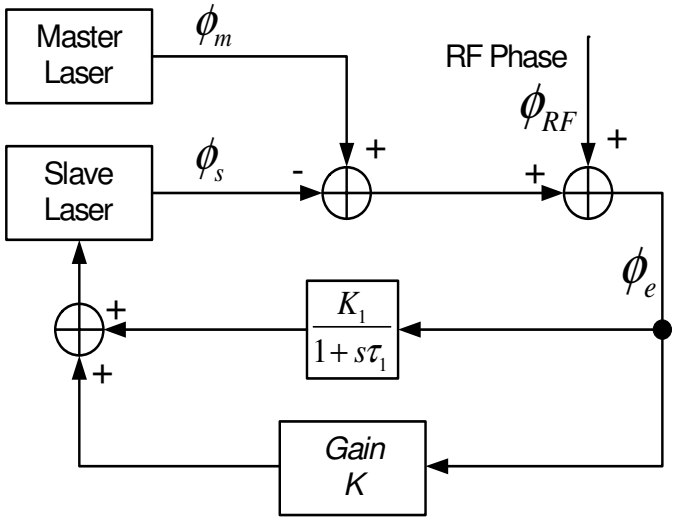

Figure 2.5. Type I, second-order OPLL using an active filter.

When a step input $\Delta\phi$ is applied, the phase error in the loop varies as

$$\phi_e(t) - \phi_{e0} = \mathcal{L}^{-1}\left(\Delta\phi \frac{s + 1/\tau_1}{s^2 + s(\frac{1}{\tau_1} + K) + \frac{K}{\tau_0}}\right). \tag{2.24}$$

Using the approximation $\tau_0^{-1} \ll \tau_1^{-1} \ll K$, this is an overdamped system, and the final solution for the phase error transient is

$$\phi_e(t) - \phi_{e0} = \Delta\phi \exp(-Kt), \tag{2.25}$$

which is identical to the simple Type I OPLL. The settling time of the loop is therefore unaffected, and the OPLL settles to (99% of) the new set-point in a time $\tau_s \simeq 4.6/K = 4 \times 10^{-7}$ s.

The loop filter described above is easily realized using passive R-C circuits [66]. The drawback of a passive filter is that additional gain has to be provided by the amplifier in the loop, which is not always feasible due to amplifier saturation. This can be overcome using an active low-pass filter in a parallel arm [66] as shown in figure 2.5. The additional branch has high DC gain ($K_1 \gg K$), and the pole is located at low frequencies so that it does not affect the loop bandwidth ($K_1/K\tau_1 \ll 1$). The

transfer function of this loop is

$$G_{op}(f) = \frac{1}{j2\pi f}\left(K + \frac{K_1}{1 + j2\pi f\tau_1}\right), \tag{2.26}$$

which is identical to equation (2.23) with $\tau_0/\tau_1 = K/K_1$.

2.2.3 Type I OPLL with Delay

We now study an OPLL in the presence of propagation delay. It must be emphasized that *all* negative feedback systems suffer from delay limitations, but the wide linewidth of SCLs makes the delay a very important factor in OPLLs, and has been studied by different authors [75, 76]. The transfer function of a delay element is given by $\exp(-j2\pi f\tau_L)$ where τ_L is the delay time. We write the open loop transfer function of a first-order loop with delay τ_L as

$$\begin{aligned} G(f) &= \frac{K_L}{jf}\exp(-j2\pi f\tau_L) \\ &= \frac{\bar{K}_L}{j\bar{f}}\exp\left(-j2\pi\bar{f}\right), \end{aligned} \tag{2.27}$$

where the normalized variables are defined as

$$\begin{aligned} \bar{f} &\doteq f\tau_L, \\ \bar{K}_L &\doteq K_L\tau_L. \end{aligned} \tag{2.28}$$

We identify the π-crossover frequency and the maximum stable gain by $\angle G(f_\pi) = -\pi$ and $|G(f_\pi)| = 1$:

$$\begin{aligned} \bar{f}_\pi &= 1/4\,, \\ \bar{K}_{L,max} &= 1/4\,. \end{aligned} \tag{2.29}$$

The loop bandwidth is therefore limited to $1/(4\tau_L)$, which is equal to the maximum hold-in range. The Bode plot for this transfer function is calculated and plotted

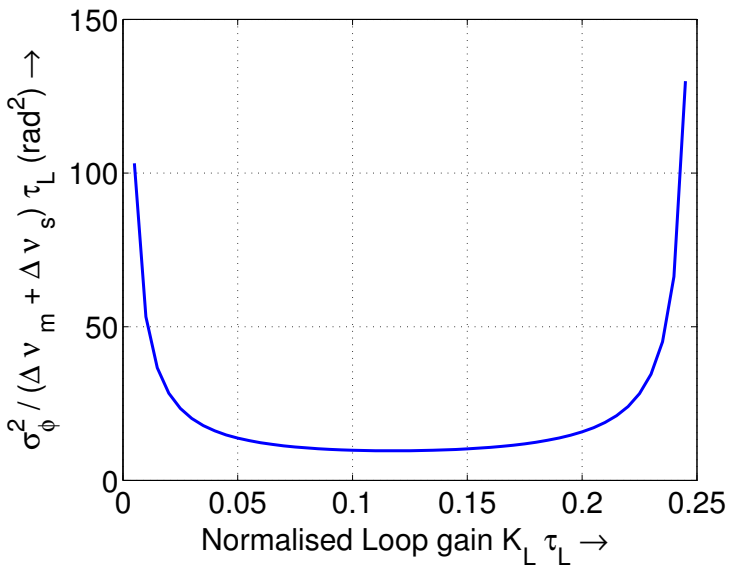

Figure 2.6. Variation of the minimum variance of the phase error as a function of the normalized gain for a Type I OPLL in the presence of propagation delay.

in figure 2.4(b), assuming a delay $\tau_L = 10$ ns, which is a typical value for optical fiber-based OPLLs. The phase crossover frequency is then equal to 25 MHz.

The variance of the residual phase error is calculated using equation (2.27) in equation (2.18) to obtain

$$\sigma_\phi^2 = \tau_L \frac{\Delta\nu_m + \Delta\nu_s}{2\pi} \int_{-\infty}^{\infty} \frac{d\bar{f}}{\bar{K}_L^2 + \bar{f}^2 - 2\bar{K}_L \bar{f} \sin(2\pi\bar{f})}. \tag{2.30}$$

The calculated value of the variance of the phase error as a function of the normalized gain is shown in figure 2.6. As expected, the phase error is very large at $\bar{K}_L = 0$ (no PLL correction) and $\bar{K}_L = 1/4$ (borderline instability). The phase error is minimum when $\bar{K}_L = \bar{K}_{L,opt} = 0.118$, and the minimum value is given by

$$\sigma_{\phi,min}^2 = 9.62\ \tau_L(\Delta\nu_m + \Delta\nu_s). \tag{2.31}$$

For a delay of 10 ns, the minimum achievable phase error is 0.05 rad^2.

2.2.4 Type II Loop with Delay

The limited hold-in range of the Type I loop of the previous loop can be improved using a lag filter design similar to section 2.2.2. Here, we consider the limiting case ($\tau_1 \to \infty$) of a Type II OPLL. In the presence of a propagation delay τ_L, the open loop transfer function is given by

$$\begin{aligned} G(f) &= -\frac{K_L(1+j2\pi f\tau_0)}{f^2}\,\exp(-j2\pi f\tau_L) \\ &= -\frac{\bar{K}_L(1+j2\pi \bar{f}\bar{\tau}_0)}{\bar{f}^2}\,\exp\left(-j2\pi \bar{f}\right), \end{aligned} \tag{2.32}$$

where the normalized variables are defined as

$$\begin{aligned} \bar{f} &\doteq f\tau_L, \\ \bar{K}_L &\doteq K_L\tau_L^2, \\ \bar{\tau}_0 &\doteq \tau_0/\tau_L. \end{aligned} \tag{2.33}$$

The π-crossover frequency is identified by setting $\angle G(f_\pi) = -\pi$, to obtain

$$\tan(2\pi\bar{f}_\pi) = 2\pi\bar{f}_\pi\bar{\tau}_0. \tag{2.34}$$

A solution to this equation exists only if $\bar{\tau}_0 > 1$, or $\tau_0 > \tau_L$. In other words, the loop is stable only if, at low frequencies, the phase lead introduced by the zero is larger than the phase lag introduced by the delay. The maximum stable loop gain is given by

$$\bar{K}_{L,max} = \frac{\bar{f}_\pi^2}{\sqrt{1+(2\pi\bar{f}_\pi\bar{\tau}_0)^2}}. \tag{2.35}$$

The variation of $\bar{f}_\pi$ and $\bar{K}_{L,max}$ as a function of the position of the loop zero $\bar{\tau}_0$ are plotted in figure 2.7, from which it is clear that the loop bandwidth approaches the limit $1/(4\tau_L)$ as $\bar{\tau}_0$ increases. *The hold-in range of this loop is infinite, owing to the presence of the pole at* $f = 0$.

We next calculate the variance of the residual phase error by plugging equation

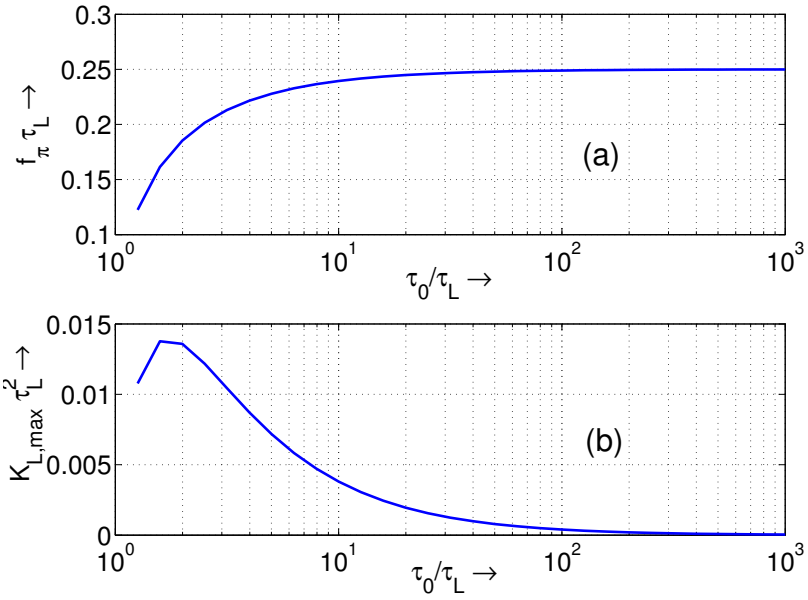

Figure 2.7. Variation of (a) the π-crossover frequency $\bar{f}_\pi$ and (b) the maximum stable loop gain $\bar{K}_{L,max}$ as a function of the position of the loop zero $\bar{\tau}_0$, for a Type II OPLL in the presence of a delay τ_L.

(2.32) into equation (2.18) to obtain

$$\sigma_\phi^2 = \tau_L \frac{\Delta\nu_m + \Delta\nu_s}{2\pi} \times \int_{-\infty}^{\infty} \frac{\bar{f}^2\, d\bar{f}}{\bar{K}_L^2 + \bar{f}^4 + 4\pi^2 \bar{K}_L^2 \bar{\tau}_1^2 \bar{f}^2 - 2\bar{K}_L \bar{f}^2 \cos(2\pi\bar{f}) - 4\pi \bar{K}_L \bar{\tau}_0 \bar{f}^3 \sin(2\pi\bar{f})}, \tag{2.36}$$

which is a function of both $\bar{\tau}_0$ and $\bar{K}_L$. As seen in the previous section, for a given value of $\bar{\tau}_0$, there is an optimum value of $\bar{K}_L$ that minimizes the variance of the phase error. For this OPLL architecture, the optimum gain is related to the maximum stable loop gain by

$$\frac{K_{L,opt}}{K_{L,max}} = 0.47\,. \tag{2.37}$$

The value of the *minimum* of the variance of the phase error as a function of $\bar{\tau}_0$ is shown in figure 2.8. As $\bar{\tau}_0$ is increased, the minimum variance of the phase error

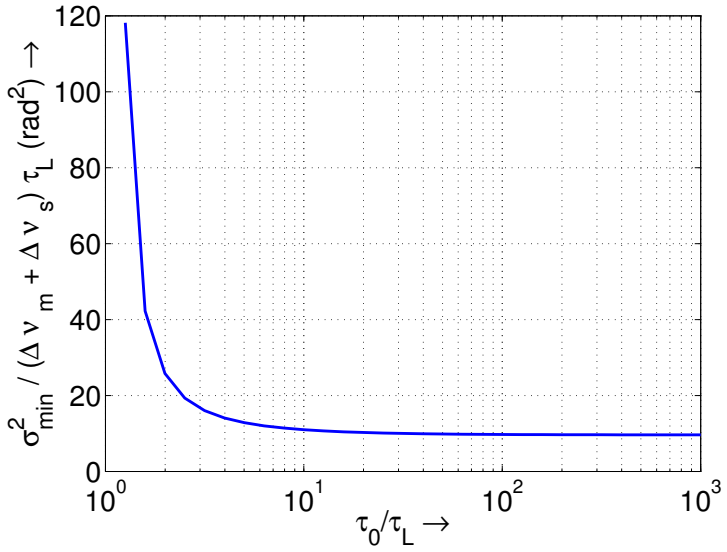

Figure 2.8. Variation of the minimum variance of the phase error as a function of the parameter $\bar{\tau_0}$, for a Type II OPLL with delay τ_L.

asymptotically reaches the value

$$\lim_{\bar{\tau_0}\to\infty} \sigma^2_{min} = 9.62\ \tau_L(\Delta\nu_m + \Delta\nu_s). \tag{2.38}$$

This result is identical to the result obtained for a first-order loop with delay in (2.31). We therefore arrive at the conclusion that in the presence of propagation delay, the performance of a second-order loop is not superior to that of a first-order loop in terms of the residual phase error. The advantage is the increased hold-in range which makes the loop insensitive to environmental fluctuations.

The settling time of OPLLs with propagation delay cannot be calculated in closed form, but is of the order of the propagation delay in the loop. It is important to minimize the loop delay in order to reduce the variance of the phase error and the settling time, and OPLLs constructed using microoptics [20] and recent efforts toward integrated OPLLs [22, 23, 77] are steps toward high-performance OPLL systems.

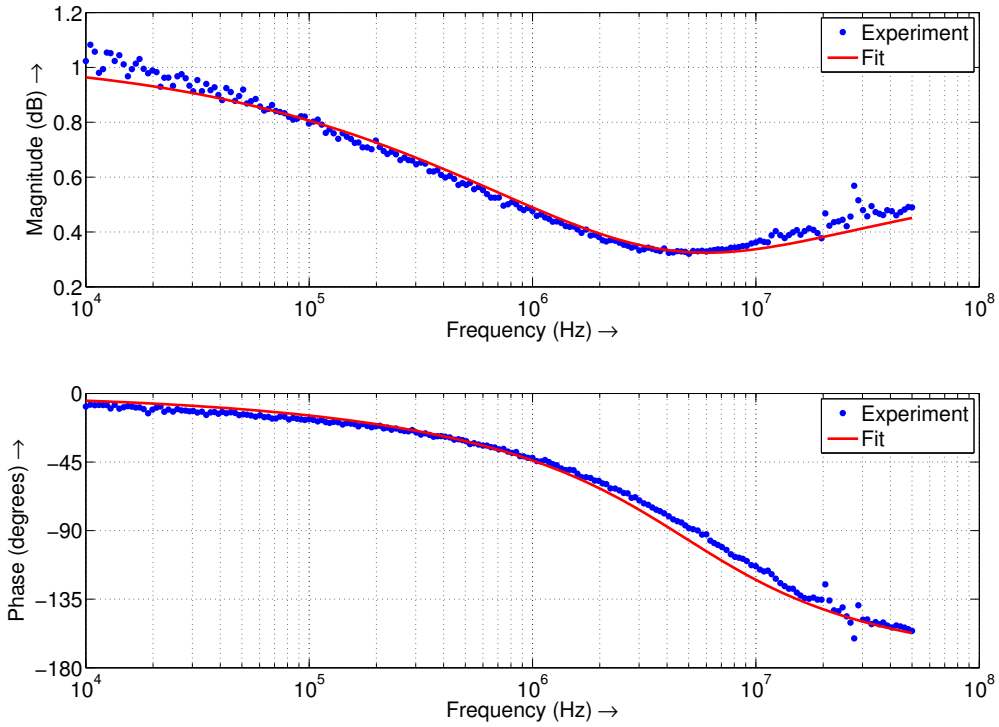

Figure 2.9. Experimentally measured FM response of a commercial DFB laser (JDS-Uniphase) with a theoretical fit using a low-pass filter model [32].

2.3 FM Response of Single-Section SCLs

We have shown that the loop propagation delay ultimately limits the achievable bandwidth and residual phase error in an OPLL, and reducing the delay is ultimately very important to achieve high-speed OPLLs. However, this discussion ignored the nonuniform frequency modulation response of the slave SCL. In practice, the biggest challenge in constructing stable OPLLs is not the propagation delay, but the SCL FM response, which limits the achievable bandwidth. The FM response of single-section SCLs is characterized by a thermal redshift with increasing current at low modulation frequencies, and an electronic blueshift at higher frequencies. This implies that at low modulation frequencies, the variation of the output optical frequency is out of phase with the input modulation, whereas the optical frequency changes in phase with the input modulation at high modulation frequencies. The FM response of the SCL therefore has a "phase reversal," which occurs at a Fourier frequency in the range of 0.1–10 MHz.

Different theoretical models have been used in literature to explain the thermal FM response of a single section SCL, including an empirical low-pass filter (LPF) response [32] and a more "physical" model based on the dynamics of heat transfer within the laser [78], [79]. In this work, we will use the empirical LPF model since it better fits the experimentally measured response of various DFB lasers, an example of which is shown in figure 2.9 for a commercially available DFB laser (JDS-Uniphase) at a wavelength of 1539 nm. The SCL FM response was measured by modulating the laser with a sinusoidal modulating current and using a Mach-Zehnder interferometer (MZI) biased in quadrature as a frequency discriminator [80]. The measurement system is calibrated using the amplitude modulation response as the baseline.

The LPF model for the FM response takes the form

$$F_{FM}(f) = K_{el} - \frac{K_{th}}{1 + \sqrt{jf/f_c}}, \tag{2.39}$$

where the first term denotes the broadband electronic response and the second term

denotes the thermal response. Note the opposite signs of the two effects—this implies that the phase of the FM response goes through a change of π radians (a "phase-reversal") as shown in figure 2.9. It is also important to note that this is a relatively "low-frequency" behavior, as opposed to high-speed free-carrier effects near the relaxation resonance frequency which have been studied more extensively [81,82]. Equation (2.39) can be rewritten in the form

$$F_{FM}(f) = \frac{1}{b}\left(\frac{b - \sqrt{jf/f_c}}{1 + \sqrt{jf/f_c}}\right), \tag{2.40}$$

where f_c denotes the corner frequency of the thermal response and depends on the device material and structure, and $b = K_{th}/K_{el} - 1$ denotes the relative strength of the thermal and electronic responses. For typical SCLs, $b > 0$, and f_c lies in the range of 0.1–10 MHz. The fit to the experimental data in figure 2.9 was obtained with $b = 1.64$ and $f_c = 1.8$ MHz.[8] A similar phase reversal was measured in a variety of single-section SCLs characterized in our lab. We will only consider $b > 0$ in this analysis, since it is the most typical case. If $b < 0$, the electronic response always dominates, and there is no phase reversal.

2.4 OPLL Filter Design

When the FM response of the SCL is included, the open-loop transfer function takes the form

$$G_{op}(f) = \frac{K}{j2\pi f}\frac{1}{b}\left(\frac{b - \sqrt{jf/f_c}}{1 + \sqrt{jf/f_c}}\right), \tag{2.41}$$

whose Bode plot is shown in figure 2.10(a) for the fitting parameters $b = 1.64$ and $f_c = 1.8$ MHz. It is clear that the FM response severely limits the phase-crossover frequency, limiting the loop bandwidth and increasing the residual phase error. This FM response limitation justifies the omission of the propagation delay in the above

[8]The fit is not very sensitive to the parameters b and f_c, and allowing for errors in experimental measurement, reasonably good fits are obtained for b in the range 1.5 to 3 and f_c between 0.7 and 2 MHz. In section 2.7, we use the values $b = 2.7$ and $f_c = 2.76$ MHz and the two curves are virtually indistinguishable.

equation; in fact, it is not possible to achieve delay-limited performance with single-section SCLs in standard OPLLs. For these fitting parameters, the minimum variance of the residual phase error can be calculated to be equal to (see appendix A)

$$\sigma^2_{min} = 8 \times 10^{-7} \left(\Delta\nu_m + \Delta\nu_s\right), \tag{2.42}$$

which yields a value of 0.4 rad^2 for a summed linewidth of 0.5 MHz.

The effect of the FM response can be somewhat mitigated using loop filters. We have developed a number of techniques to improve loop performance, and these are described in detail in reference [73]. We will here describe the salient features of our filter design. Firstly, a lead filter is used to push the phase-crossover frequency to higher frequencies, as shown in the Bode plot in figure 2.10(b). Such a filter has the form

$$F_f(f) = \frac{1 + j2\pi f\tau_2}{1 + j2\pi f\tau_3}, \tag{2.43}$$

with $\tau_2 > \tau_3$, and the values $\tau_2 = 10^{-7}$s and $\tau_3 = 10^{-9}$s were used in the calculation. The use of the lead filter reduces the minimum variance of the phase error from ∼0.4 to ∼0.2 rad^2. This value is in reasonable agreement with the experimentally measured residual phase error of 0.12 rad^2 for an optimized OPLL with this SCL (see section 2.5).[9]

An OPLL using a single-section SCL therefore requires that the SCL linewidth should be very narrow (<1 MHz), and a lead filter is necessary to improve the loop bandwidth. The hold-in range of the OPLL is still limited by the low DC gain of a Type I OPLL, and we therefore add a lag filter at low frequencies to increase the hold-in range, as analyzed in section 2.2.2. A practical SCL-OPLL configuration is therefore described in figure 2.11, and we have experimentally demonstrated an increase in the hold-in range from ∼10 MHz to ∼3.5 GHz using this configuration.

[9] An important cause of the discrepancy between theory and experiment is the assumption of a Lorenzian lineshape for the laser—it is shown in chapter 3 that this slave SCL has a significant amount of $1/f$ noise at low frequencies, which contributes to the measured free-running linewidth, but is very well corrected by the OPLL leading to a smaller residual phase error.

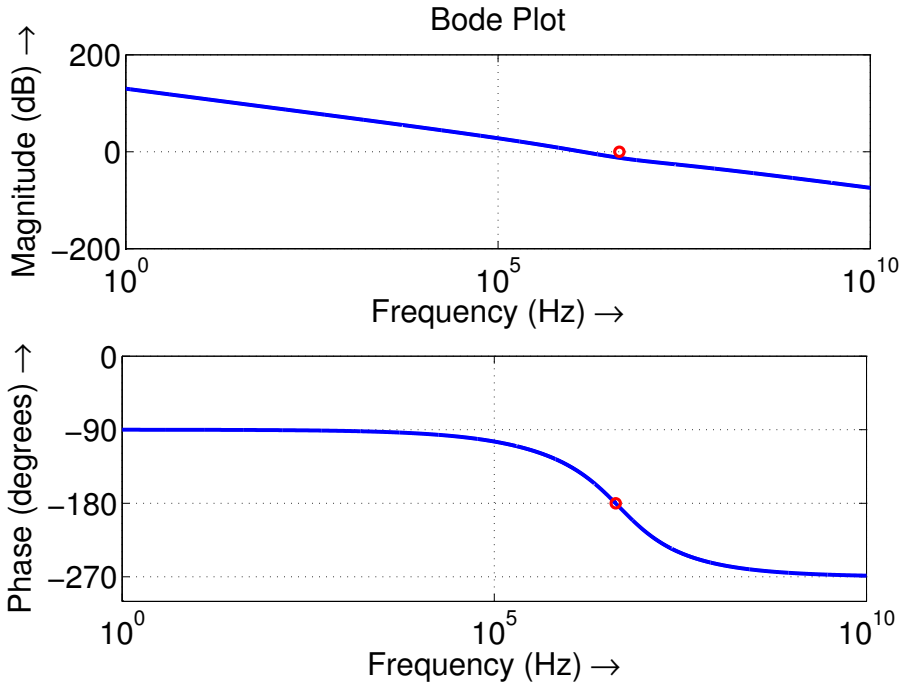

(a)

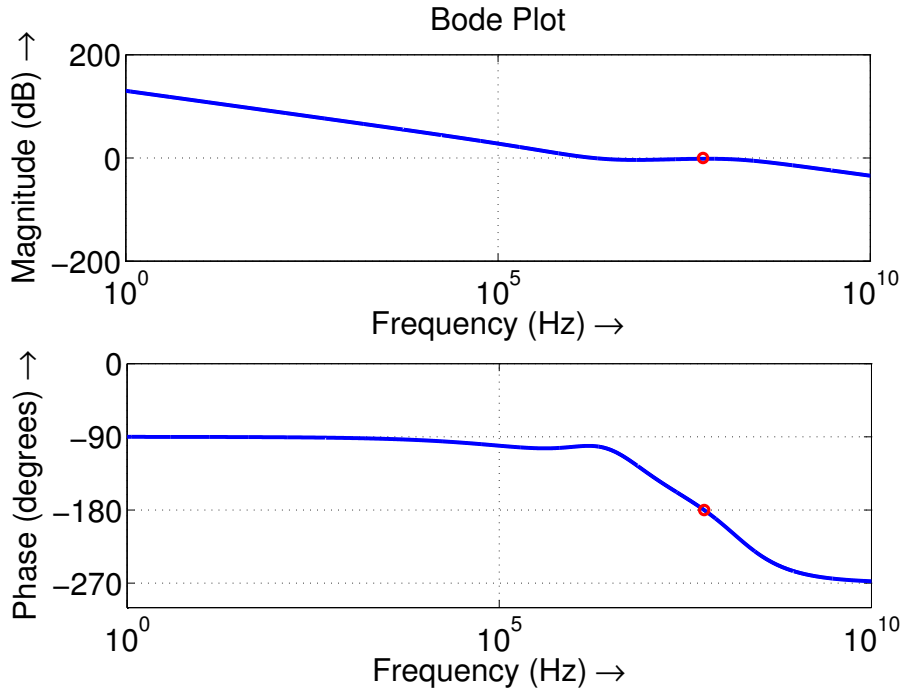

(b)

Figure 2.10. Bode plots for (a) a Type I OPLL including the SCL FM response, and (b) the same response with an additional lead filter. The lead filter pushes the phase-crossover frequency (indicated by the marker) to higher frequencies, enabling a larger loop bandwidth.

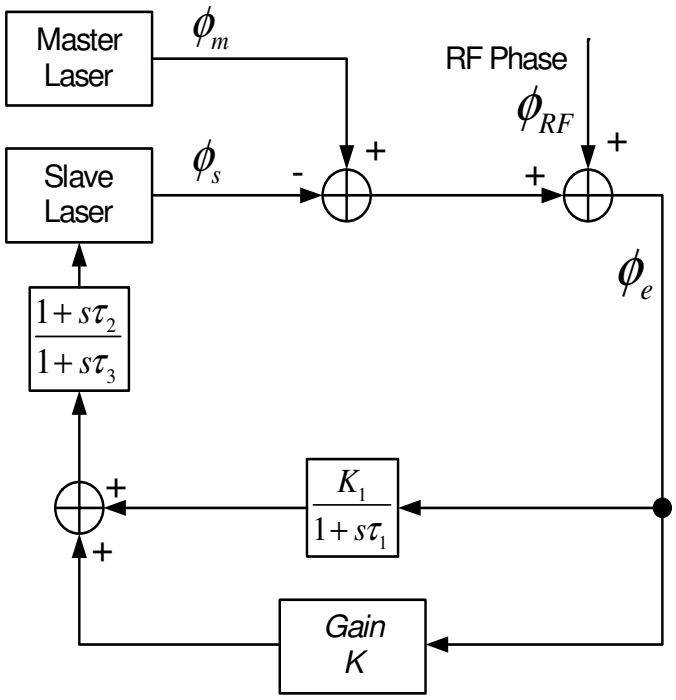

Figure 2.11. Practical OPLL configuration, including a lead filter to increase the phase-crossover frequency and a low frequency active lag filter (implemented by the parallel arm) to increase the hold-in range.

2.5 Phase-Locking of Commercial SCLs

We phase-locked a number of commercially available SCLs of different types and operating wavelengths in the heterodyne OPLL configuration shown in figure 2.1. We present phase-locking results of five different SCLs in table 2.1: a DFB laser at 1539 nm (JDS-Uniphase Corp., Milpitas, CA), an external cavity SCL at 1064 nm (Innovative Photonic Solutions, Monmouth Junction, NJ), a high power master-oscillator power amplifier (MOPA) SCL at 1548 nm (QPC Lasers, Sylmar, CA), a vertical external cavity surface-emitting laser (VECSEL) at 1040 nm (Novalux, Sunnyvale, CA, with a home-built external cavity) and a DFB laser at 1310 nm (Archcom Tech., Azusa, CA). The temperature of the slave SCLs was controlled to within 0.01 °C using a thermoelectric cooler. Different master lasers were used in the experiments. The outputs of the fiber-coupled slave and master lasers were combined using a fiber coupler, and a high speed PD (NewFocus 1544-B) was used to detect the beat note between the lasers. A tunable RF oscillator with linewidth $\ll$ 10 kHz was used as

Table 2.1. Parameters of OPLLs demonstrated using commercially available SCLs

Slave SCL	λ (nm)	SCL power	SCL 3 dB linewidth	Master Laser	σ_ϕ^2 (rad^2)
DFB[a]	1539	60 mW	0.5 MHz	Fiber Laser[h]	0.11
Ext. cavity[b]	1064	100 mW	0.2 MHz	Fiber Laser[h]	0.014
MOPA[c]	1548	1000 mW	0.5 MHz	Tunable Laser[i]	0.08
VECSEL[d]	1040	40 mW	<0.01 MHz[f]	VECSEL[d]	0.007
DFB[e]	1310	5 mW	∼0.5 MHz[g]	DFB SCL[e]	0.2

[a] JDS-Uniphase Corp.
[b] Innovative Photonic Solutions.
[c] QPC Lasers.
[d] Novalux, with home-built cavity.
[e] Archcom Tech.
[f] This is an estimate, the actual linewidth was too low to be measured by the self-heterodyne technique.
[g] Measured by beating two similar DFB lasers.
[h] NP Photonics, Tucson, AZ, linewidth ∼30 kHz.
[i] Agilent, linewidth ∼50 kHz.

the offset signal. Discrete RF amplifiers and mixers (MiniCircuits, Brooklyn, NY) were used to provide gain and mix the RF signals. The DC current and the temperature of the slave SCL were adjusted to bring the free-running frequency difference between the master and slave SCLs to within the loop acquisition range. The total propagation delay in the loop was estimated to be of the order of 10 ns. Filters were used to increase the loop hold-in range and bandwidth as described in the previous section, and stable phase-locking for at least 30 minutes was observed.

The phase-locking performance was characterized by measuring a part of the loop PD output using a high speed spectrum analyzer, and the results are shown in figure 2.12. The offset RF frequency, which ranged from 0.8 to 1.7 GHz in these experiments, is subtracted from the x-axis. If the phase-locking is perfect, this signal is a pure tone at the frequency $\omega_s - \omega_m = \omega_{RF}$ (zero in the figure). However, imperfect phase-locking leads to a residual phase error which shows up as wings in the spectrum. This beat

signal is given by

$$V_{beat} \propto \cos(\omega_{RF}t + \phi_{RF}(t) + \phi_e(t)). \tag{2.44}$$

Since the phase noise of the RF source is negligible and the variance of the phase error ϕ_e is much smaller than 1 rad^2 in lock, the spectrum of the beat signal is directly proportional to the spectral density of the phase error, offset by the RF frequency, i.e.

$$V_{beat} \propto \cos(\omega_{RF}t) - \sin(\omega_{RF}t) \times \phi_e(t). \tag{2.45}$$

The first term is the ideal result with no phase error, leading to a delta function in the spectrum, while the spectrum of the second term is the spectral density of the phase error. The variance of the phase error, which is the integral of the spectral density, is therefore calculated by integrating the "noise" spectrum of the beat signal. Defining the "phase-locking efficiency" η as the ratio of coherent power (area under the delta function) to the total power (coherent power + noise power), we can write down

$$\eta = \frac{1}{1 + \langle \phi_e^2(t) \rangle} = \frac{1}{1 + \sigma_\phi^2}, \tag{2.46}$$

so that

$$\sigma_\phi^2 = \frac{1}{\eta} - 1. \tag{2.47}$$

The calculated standard deviations of the phase error for the different OPLLs are indicated in figure 2.12, and the variances are listed in table 2.1.

The linewidths of the slave SCLs were measured, wherever possible, using a delayed self-heterodyne interferometer with interferometer delay time much larger than the laser coherence time [83]. The laser output was split into two parts, and one arm was phase modulated using an external optical phase modulator to generate sidebands. The other arm was delayed by a delay time longer than the laser coherence time. The beat between this delayed signal and one of the phase-modulated sidebands yields a lineshape with linewidth equal to twice the linewidth of the SCL. The phase-locking results in figure 2.12 and table 2.1 show, unsurprisingly, that SCLs with narrower linewidths have lower residual phase errors in their OPLLs.

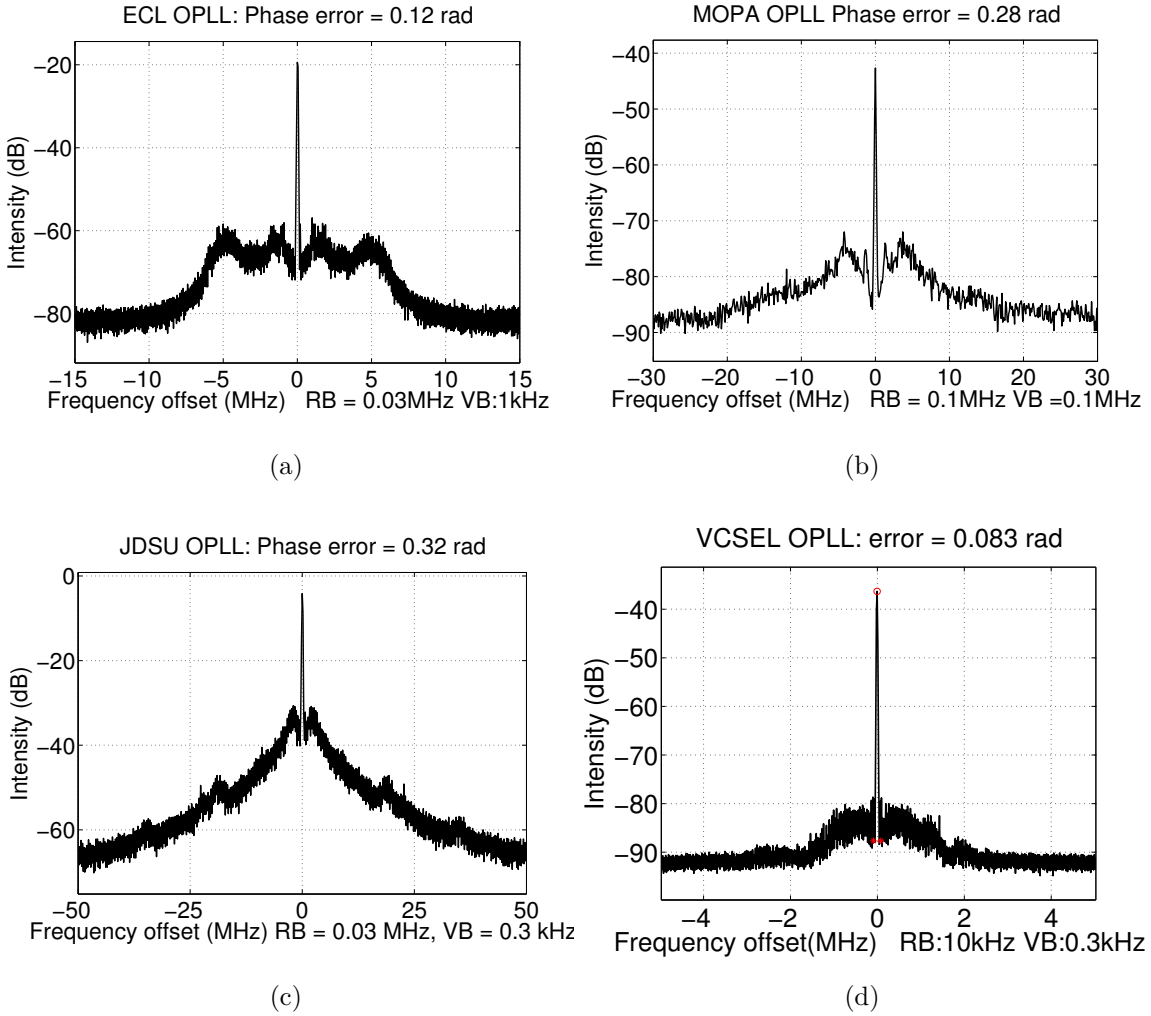

Figure 2.12. Phase-locking results using various commercially available SCLs. The standard deviation of the residual phase error in each OPLL is indicated, along with the resolution and video bandwidths of the measurement. (a) External cavity SCL (Innovative Photonic Solutions), (b) MOPA SCL (QPC Lasers), (c) DFB SCL (JDS-Uniphase Corp.), (d) VECSEL (Novalux, home-built). Other OPLL parameters are given in table 2.1.

In addition to the discrete-electronics-based SCL-OPLLs demonstrated in this section, integrated electronic circuits were developed by our collaborators at the University of Southern California for phase-locking [84]. This circuit also included an aided acquisition module which enables the automatic tuning of the SCL bias current in order to bring its free-running frequency to within the acquisition range of the OPLL.

While we have succeeded in phase-locking a number of commercial OPLLs, the standard OPLL architectures described above still impose stringent requirements on the SCL linewidth. We would like to reduce the residual phase error to even smaller numbers than reported in table 2.1. Further, it was not possible to phase-lock a number of other commercially available SCLs, and we would like to develop techniques to enable phase-locking of *any* SCL. Two such techniques have been developed as part of this work, and are described in the next two sections, namely, sideband locking (section 2.6) and composite OPLLs (section 2.7).

2.6 Novel Phase-Lock Architectures I: Sideband Locking

We have shown in the previous sections that for stable loop operation, it is necessary that the loop bandwidth be much larger than the summed linewidths of the two lasers. The maximum achievable bandwidth of an OPLL is ultimately limited by the loop propagation delay, but a more stringent limitation on the loop bandwidth is imposed by the phase reversal in the FM response $F_{FM}(f)$ of single section SCLs. The traditional solution to this problem has been the use of multielectrode SCLs [17–20], but they do not offer the robustness and simplicity of operation of single-section DFB SCLs. Other approaches to overcome the thermal-induced bandwidth limitation have included the use of external cavity SCLs with narrow linewidths [11–16] or the use of an additional optical injection locking loop [85–87] or external optical modulators for phase-locking [34, 35]. Most of these methods require the use of very specialized

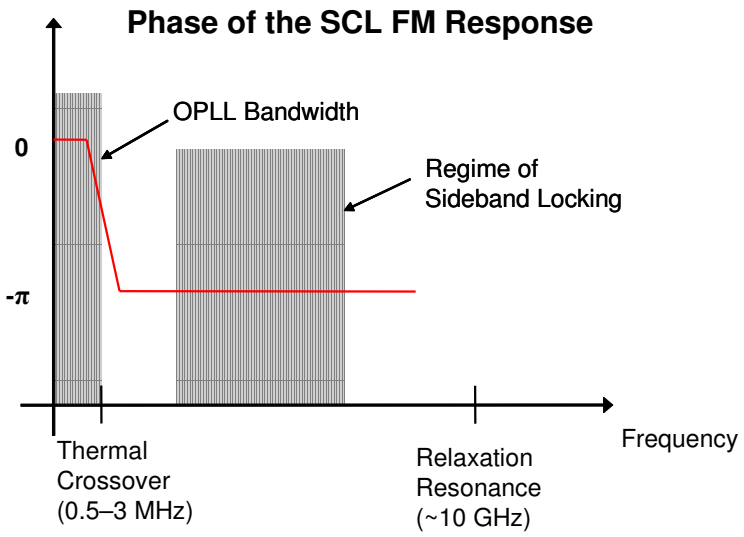

Figure 2.13. Cartoon representation of the phase response of a single-section SCL showing the regimes of operation of a conventional OPLL and a sideband-locked OPLL.

lasers or complicated optical feedback systems. In this section, we demonstrate that the limitation imposed by the phase reversal of the FM response of a single-section SCL can be eliminated using a sideband-locked heterodyne OPLL, which reduces system complexity when compared to other approaches, and *enables delay-limited SCL-OPLLs using most readily available SCLs.*

2.6.1 Principle of Operation

The FM response of a single section SCL is determined by a thermal redshift at low frequencies and an electronic blueshift at higher frequencies, leading to a dip in the amplitude response and a phase reversal at a few megahertz [78]. At frequencies between this crossover frequency and the relaxation resonance frequency of the laser ($\sim$10 GHz), the amplitude and phase of the FM response are constant. If the feedback current into the SCL is upshifted into this frequency range, a much wider frequency range is opened up for phase-locking, and loop bandwidths of up to a few GHz are achievable. This is depicted pictorially in figure 2.13.

Consider the heterodyne sideband-locked OPLL system shown in figure 2.14. A part of the SCL output is combined with the master laser using a 2×1 fiber coupler,

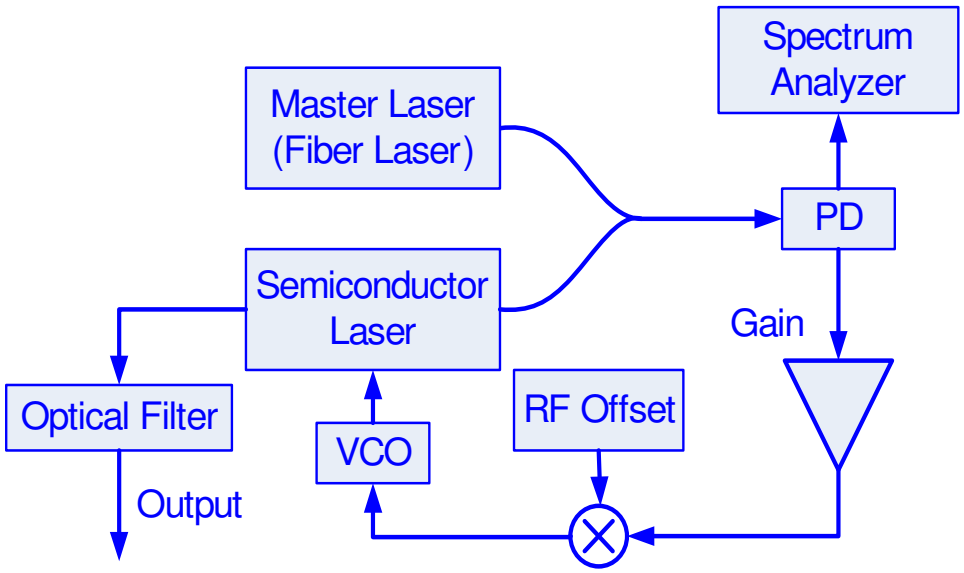

Figure 2.14. Schematic diagram of a heterodyne sideband-locked OPLL.

and mixed in a high speed PD. The error signal at the output of the PD is mixed with an RF offset signal, filtered, and fed into a voltage-controlled oscillator (VCO). The phase and frequency of the VCO are denoted by ω_v and ϕ_v respectively. The VCO output is in turn fed into the SCL, creating multiple FM sidebands whose frequency and phase in the free-running condition are given by

$$\begin{aligned} \omega_{s,k} &= \omega_s^{fr} + k\omega_v, \\ \phi_{s,k} &= \phi_s^{fr} + k\phi_v, \end{aligned} \tag{2.48}$$

with $k = 0, \pm 1, \pm 2, \ldots$. Any one of these sidebands can now be locked to the master laser. Assume the nth sideband is phase-locked to the master laser. The frequency and phase of this locked sideband are given by

$$\begin{aligned} \omega_{s,n}^{\text{lock}} &= \omega_m + \omega_{RF}, \\ \phi_{s,n}^{\text{lock}} &= \phi_m + \phi_{RF}. \end{aligned} \tag{2.49}$$

It is important to note that while the locked nth sideband is coherent with the master laser, the other sidebands are necessarily incoherent. This is clear from equation (2.48), where the phase correction provided by the VCO is different for different

sideband orders. The other sidebands therefore have to be optically filtered out, as shown in figure 2.14. The power in the nth sideband (normalized to the total optical power) is given by

$$P_n = \left| J_n \left(\frac{|F_{FM}(\omega_v/2\pi)|\, A_v}{\omega_v} \right) \right|^2, \tag{2.50}$$

where J_n is the n^{th} order Bessel function of the first kind, and A_v is the amplitude of the modulating current at the VCO output. In order to maximize the total coherent power, the $n = 1$ sideband is phase-locked, and the amplitude A_v is chosen so as to maximize the power in the first sideband. From equation (2.50), at the optimal value of A_v, 33.6% of the total power is in the first sideband. This power penalty introduced by the filtering of the incoherent sidebands is acceptable in most applications of OPLLs owing to the high output power of the SCLs.

The open-loop transfer function of the system shown in figure 2.14, with respect to the phase of the first optical FM sideband is given by

$$G_1(f) = \frac{K_1 F_{FM}^{VCO}(f) F_f(f) e^{-j2\pi f \tau_L}}{j2\pi f}, \tag{2.51}$$

where K_1 is the open-loop DC gain and $F_{FM}^{VCO}(f)$ is the normalized FM response of the VCO. Equation (2.51) is valid whenever the nominal VCO frequency is chosen to be in the frequency range where the FM response of the SCL is constant. The loop bandwidth is therefore constrained by the FM bandwidth of the VCO and the loop propagation delay, *and is independent of the thermal FM response of the laser*. If a high-bandwidth VCO is used, the loop bandwidth is limited primarily by the propagation delay in the loop, which is what we set out to achieve in this section.

2.6.2 Experimental Demonstration

The sideband locking experiment was demonstrated using a commercially available fiber coupled DFB SCL (Archcom Tech.) with an output power of 40 mW at 1550 nm, and a tunable master laser with a linewidth of ∼50 kHz. The loop PD had a bandwidth of 12 GHz. The measured FM response of the SCL, shown in figure 2.15,

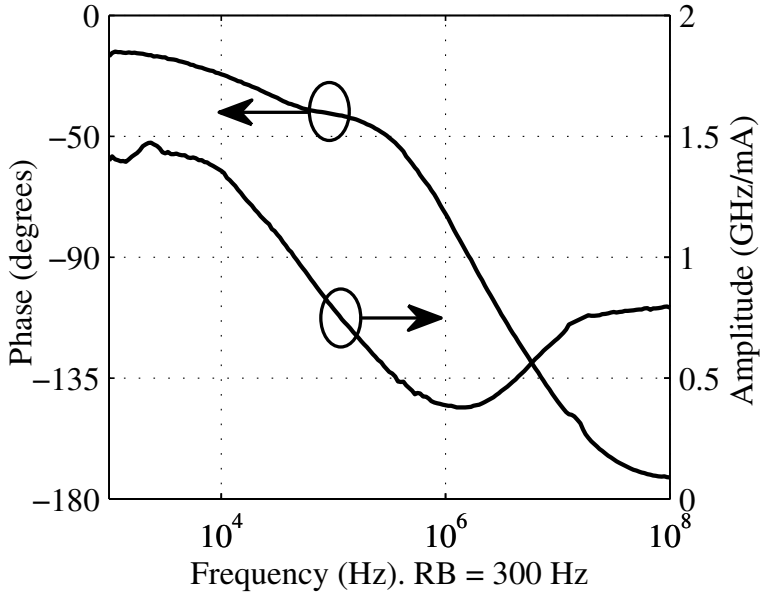

Figure 2.15. Measured FM response of the DFB SCL used in the sideband locking experiment.

exhibits a $\pi/2$ phase-crossover at a frequency of 1.6 MHz, which is lesser than its 3 dB linewidth of 5 MHz; and *the SCL therefore could not be phase-locked in the simple heterodyne OPLL of figure 2.1.* However, using the sideband-locking technique presented in this section, the first FM sideband of this SCL was successfully phase-locked to the master laser in a fiber-based OPLL using discrete RF electronic components. The frequencies of the VCO and the RF offset signal were chosen to be 4 GHz and 1.5 GHz respectively. The locked FM sideband was optically filtered using a Fiber Bragg Grating with a narrow 20 dB bandwidth of 10 GHz (Orbits Lightwave, Pasadena, CA). A suppression ratio of >25 dB to the carrier and the $n = 2$ sideband was achieved in the filtered output.

The bandwidth of the fiber-based OPLL without a loop filter was about 20 MHz, corresponding to a total loop propagation delay of 12.5 ns. By varying the fiber delay in the loop, it was verified that the bandwidth was limited by the loop delay. A

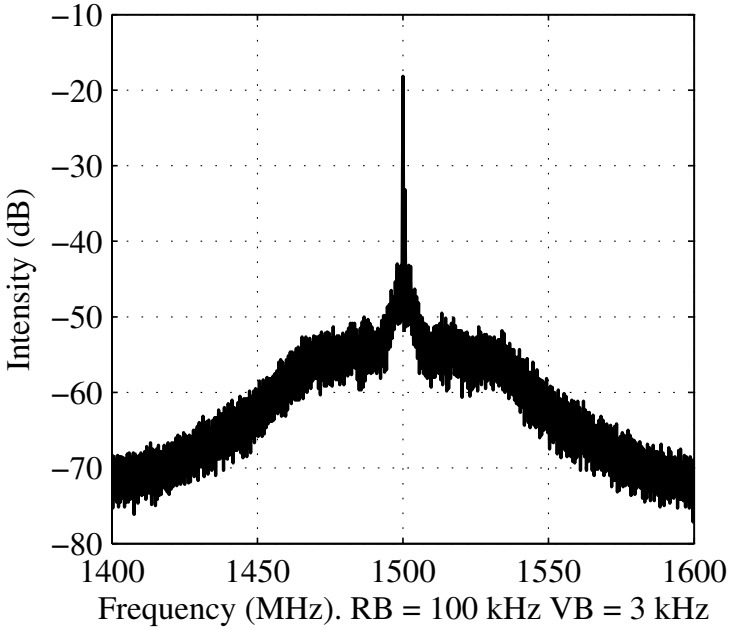

Figure 2.16. Beat spectrum between the locked sideband of the slave SCL and the master laser.

passive R-C filter with the transfer function

$$F_f(f) = \frac{(1 + j2\pi f\tau_{z1})(1 + j2\pi f\tau_{z2})}{(1 + j2\pi f\tau_{p1})(1 + j2\pi f\tau_{p2})} \tag{2.52}$$

was used in the loop to improve the bandwidth, with $\tau_{z1} = 53.6$ ns, $\tau_{z2} = 1.41$ µs, $\tau_{p1} = 4.34$ ns and $\tau_{p2} = 8.71$ µs. The resultant loop bandwidth was measured to be 35 MHz and the hold-in range was ±90 MHz. The measured spectrum of the beat signal between the phase-locked FM sideband and the master laser is shown in figure 2.16. The locking efficiency η is calculated from the spectrum to be 80%. This corresponds to a residual phase error variance of $\sigma_\phi^2 = 0.25\ \text{rad}^2$. The loop bandwidth and the residual phase error can be further improved by reducing the loop propagation delay.

The lineshape of the master laser and that of the filtered $n = 1$ sideband of the slave SCL, measured using the delayed self-heterodyne interferometer technique, are shown in figure 2.17. The lineshape of the locked SCL sideband follows that of the master laser for frequencies within the loop bandwidth, and reverts to the unlocked

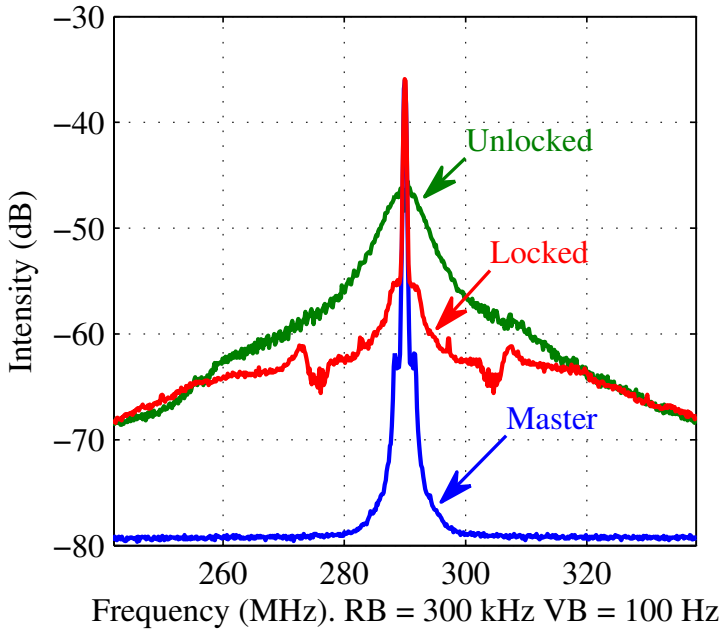

Figure 2.17. Lineshape measurements of the master laser, free-running and phase-locked optical sideband of the slave SCL, using a delayed self-heterodyne interferometer with a frequency shift of 290 MHz.

lineshape outside the loop bandwidth.

In summary, the limitation imposed on the loop bandwidth of an OPLL using a single section DFB SCL by the phase reversal of the laser FM response can be overcome by locking an FM sideband of the SCL to the master laser. Using this technique, the sideband locking of a DFB laser, which could not be locked in a simple heterodyne OPLL, was demonstrated. A delay-limited bandwidth of 35 MHz was achieved, which can be increased to a few hundreds of megahertz using miniature or integrated optics and integrated RF electronic circuits. The phase-locked sideband was optically filtered, and it was shown that the phase noise of the filtered locked sideband was determined by that of the master laser for frequencies within the loop bandwidth. The demonstrated approach to phase-locking SCLs facilitates the phase-locking of standard single section DFB SCLs with moderately large linewidths, with very little increase in system complexity.

2.7 Novel Phase-Lock Architectures II: Composite OPLLs

The sideband locking approach developed in section 2.6 can be used to phase-lock SCLs with large linewidths, but it comes with two drawbacks: (i) only a third of the SCL output power is useful coherent power, and (ii) a narrow-band optical filter is necessary to filter out the coherent optical sideband. While these restrictions are acceptable in most applications, there are some others, such as OPLLs where the frequency of the slave SCL needs to be tuned, where the use of the optical filter is undesirable. In this section, we demonstrate an alternative solution that involves the use of an optical phase modulator to extend the bandwidth of the loop and reduce the residual phase error. The basic idea behind the approach is to use the phase modulator to provide correction at higher frequencies where the thermal response of the SCL is negligible. We demonstrate theoretically and experimentally the improvement of loop bandwidth using two different loop configurations. The use of discrete optical and electronic components in our proof-of-principle experiment results in a reduction of the residual phase noise by about a factor of two; however, the use of integrated optical phase modulators in photonic integrated circuits [22, 77] can lead to very efficient OPLL systems.

2.7.1 System Description

2.7.1.1 Double-Loop Configuration

Consider the schematic diagram of the control system shown in figure 2.18(a). The SCL is first phase-locked to the master laser in a heterodyne OPLL; this loop is shown with the photodetector PD1 in the figure. The output of the phase-locked SCL is phase modulated and mixed with the master laser in a second photodetector PD2. The resultant error signal is down-converted, filtered, and input to the phase modulator. The output of the phase modulator serves as the useful optical output. The linearized small-signal model for the propagation of the optical phase in the

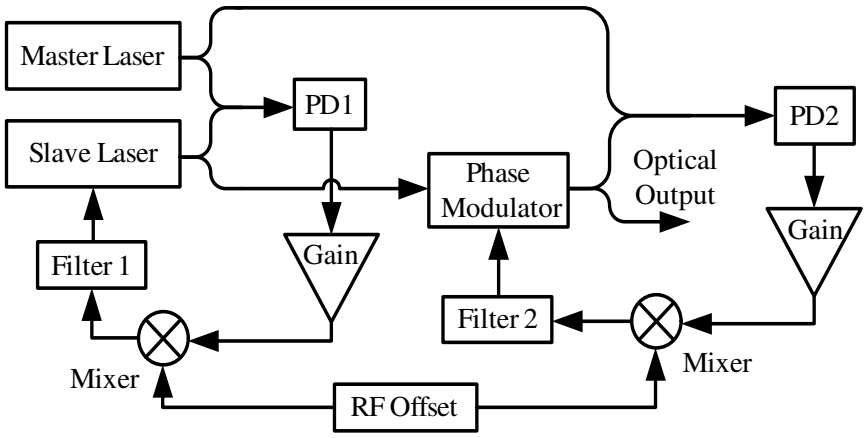

(a)

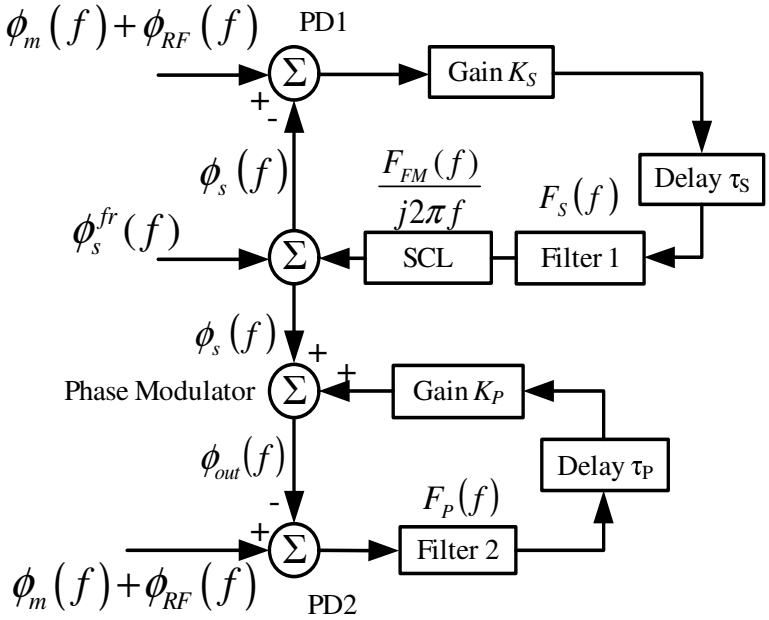

(b)

Figure 2.18. (a) Schematic diagram of the double-loop configuration. (b) Linearized small-signal model for phase propagation. PD1 and PD2 are photodetectors.

frequency domain is shown in figure 2.18(b). The DC gain K_P is the product of the gains of the photodetector, mixer, loop amplifier, filter, and the phase modulator. The filter transfer function $F_P(f)$ is assumed to be normalized to unity. For notational simplicity, in this section, we will denote the open-loop transfer function of the simple OPLL (equation (2.10))as $G(f)$ and drop the subscript *op*, and refer to the summed laser linewidth as $\Delta\nu \doteq \Delta\nu_m + \Delta\nu_s$.

This system can simply be analyzed as two separate feedback loops in series. The phase $\phi_s(f)$ of the output of the slave laser locked to the master laser is given by equation(2.12). The open-loop transfer function of the second loop is given by

$$G_P(f) = K_P F_P(f) \exp(-j2\pi f \tau_P). \tag{2.53}$$

The output phase $\phi_{out}(f)$ is related to $\phi_s(f)$ by

$$\phi_{out}(f) = \frac{G_P(f)}{1+G_P(f)}\left(\phi_m(f) + \phi_{RF}(f)\right) + \frac{1}{1+G_P(f)}\phi_s(f), \tag{2.54}$$

which, using equation (2.12), reduces to

$$\phi_{out}(f) = \left[\frac{G_P}{1+G_P} + \frac{G}{(1+G)(1+G_P)}\right](\phi_m + \phi_{RF}) + \frac{1}{(1+G)(1+G_P)}\phi_s^{fr}, \tag{2.55}$$

where we have omitted the argument f. The spectral density of the residual phase error $\phi_e = \phi_s - \phi_m - \phi_{RF}$ is therefore given by

$$S_\phi^e(f) = \frac{\Delta\nu}{2\pi f^2}\left|\frac{1}{(1+G(f))(1+G_P(f))}\right|^2, \tag{2.56}$$

and the variance of the phase error is

$$\sigma_\phi^2 = \int_{-\infty}^{\infty} \frac{\Delta\nu}{2\pi f^2}\left|\frac{1}{(1+G(f))(1+G_P(f))}\right|^2 df. \tag{2.57}$$

Comparing equations (2.18) and (2.57), we see that the addition of the second feedback loop causes a reduction in the phase error at frequency f by a factor $|1/(1+$

$G_P(f))|$, and the bandwidth over which the phase noise is reduced can be extended to beyond that of the conventional OPLL, up to the propagation delay limit.

In the preceding analysis, we have made the assumption that the optical path lengths from the master laser and the phase-locked slave laser to the photodetector PD2 are equal, so that the detector is biased at quadrature. (Note that the OPLL forces the two optical fields at PD1 to be in quadrature.) In practice, path length matching may be difficult to achieve without the use of photonic integrated circuits, and this represents a potential drawback of this approach. Further, variations in the relative optical path lengths result in changes in the gain seen by the second feedback loop, resulting in larger residual phase errors. This issue is addressed in the composite OPLL configuration discussed in the next section.

2.7.1.2 Composite PLL

The need for precise optical path length matching is eliminated in the composite PLL architecture shown in figure 2.19(a), where the phase error measurement is performed at a single photodetector PD. This phase error is split into two paths, one of which drives the SCL as in a conventional OPLL, whereas the second path is connected to the input of the optical phase modulator. The output of the phase modulator serves as the useful optical output. The linearized small-signal model for this composite PLL is shown in figure 2.19(b). The gain K_P is again defined here as the product of the DC gains of the photodetector, amplifier, mixer, and Filter 2. This feedback system can be regarded as comprising an integrating path (SCL) and a proportional path (phase modulator). The integral path has large gain only over a limited frequency range, but this is sufficient to track typical frequency drifts of the lasers.

Defining the open-loop transfer functions of the two feedback paths as

$$\begin{aligned} G(f) &= \frac{K_S F_{FM}(f) F_S(f) \exp[-j2\pi f(\tau_1+\tau_2)]}{j2\pi f}, \\ G_P(f) &= K_P F_P(f) \exp(-j2\pi f \tau_2), \end{aligned} \tag{2.58}$$

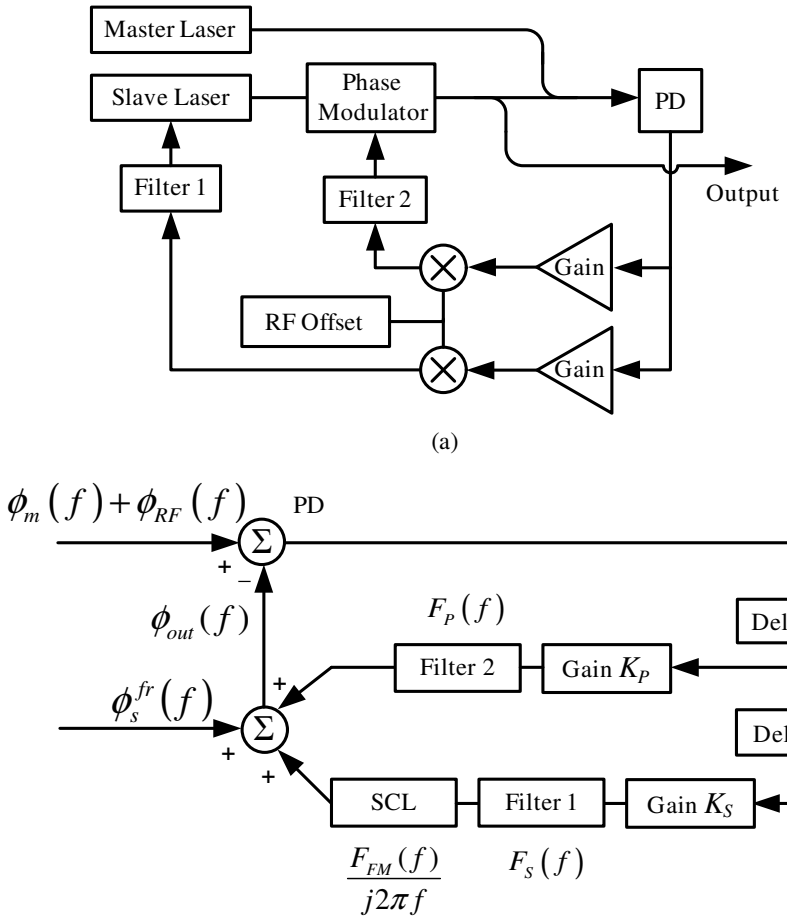

Figure 2.19. (a) Schematic diagram of the composite heterodyne OPLL. (b) Linearized small-signal model for phase propagation. PD: Photodetector.

the output phase is given by

$$\phi_{out}(f) = \frac{G(f)}{1 + G(f) + G_P(f)} \left(\phi_m(f) + \phi_{RF}(f)\right) + \frac{1}{1 + G(f)} \phi_s^{fr}(f), \tag{2.59}$$

and the variance of the residual phase error $\phi_e = \phi_{out} - \phi_m - \phi_{RF}$ is

$$\sigma_\phi^2 = \int_{-\infty}^{\infty} \frac{\Delta\nu}{2\pi f^2} \left| \frac{1}{1 + G(f) + G_P(f)} \right|^2 df. \tag{2.60}$$

The function $G_P(f)$ is chosen so that, at frequencies larger than the FM crossover frequency of the SCL, where the function $G(f)$ exhibits a phase reversal, the gain in the phase modulator arm $G_P(f)$ dominates over the gain in the SCL arm $G(f)$. This ensures phase correction over a larger frequency range, thereby leading to a reduced phase error between the output optical wave and the master laser.

2.7.2 Results

2.7.2.1 Laser Frequency Modulation Response

Two commercial single-mode distributed feedback lasers operating at a wavelength of 1539 nm (JDS-Uniphase) were used in the experimental demonstration. The lasers had a 3 dB linewidth of ∼0.5 MHz, and their frequency modulation response exhibited the characteristic phase crossover at a frequency of ∼5 MHz as shown in figure 2.20. The FM responses of the two lasers were very similar, and only one curve is shown for clarity. The theoretical fit to the FM response using equation (2.40) is also shown, with fitting parameters $b = 2.7$ and $f_c = 0.76$ MHz.

2.7.2.2 Numerical Calculations

The spectral density of the residual phase error in the loop, and its variance, were numerically calculated for each of the three system configurations shown in figures 2.1, 2.18 and 2.19, using equations (2.18), (2.56) and (2.60) respectively. For the sake of simplicity, the SCL was assumed to have a Lorenzian lineshape (white frequency noise spectrum) with a 3 dB linewidth of 200 kHz, and an FM response as modeled

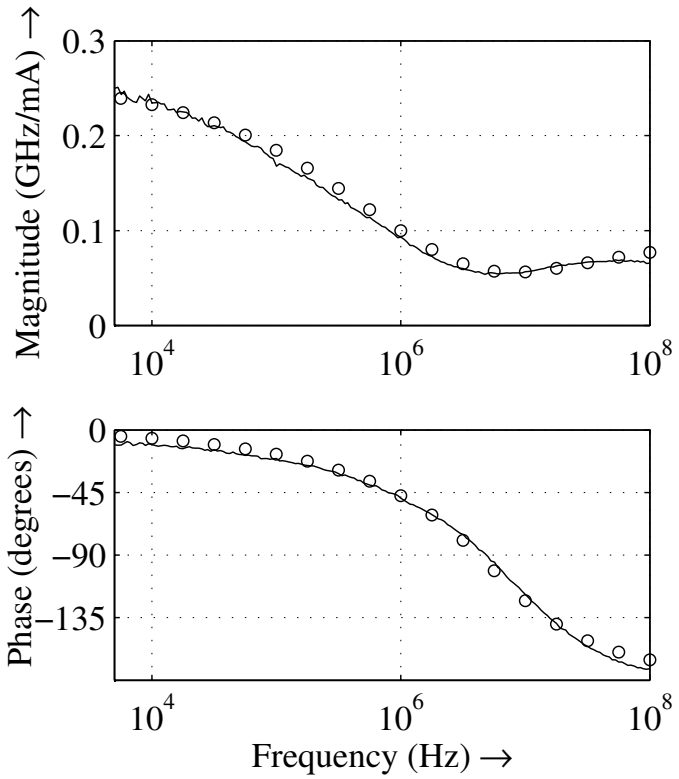

Figure 2.20. Experimentally measured frequency modulation of a single-section distributed feedback semiconductor laser (solid line) and theoretical fit using equation (2.40) (circles).

in the preceding section. The experimentally measured linewidth of the laser is larger than this value, owing to the deviation of the frequency noise spectrum from the ideal white noise assumption (chapter 3, [63]). The propagation delay in each path was assumed to be 8 ns, i.e., $\tau_S = \tau_P = \tau_1 = \tau_2 = 8$ ns. This value was chosen to be a representative value for OPLLs constructed using fiber-optics and discrete electronic components. The parameters of the loop filters were chosen to match the values of the lag filters used in the experiment. The filter transfer functions were given by

$$F_S(f) = \frac{1 + j2\pi f\tau_{Sz}}{1 + j2\pi f\tau_{Sp}}, \tag{2.61}$$

with $\tau_{Sz} = 24$ µs and $\tau_{Sp} = 124$ µs; and

$$F_P(f) = \frac{1 + j2\pi f\tau_{Pz}}{(1 + j2\pi f\tau_{Pp1})(1 + j2\pi f\tau_{Pp2})^2}, \tag{2.62}$$

with $\tau_{Pz} = 15$ ns, $\tau_{Pp1} = 1.3$ µs, and $\tau_{Pp2} = 0.8$ ns. The double-pole at $1/(2\pi\tau_{Pp2}) =$ 200 MHz approximates the finite bandwidth of the op-amp used to construct the filter in the experiment.

With the above parameters, the value of K_S was optimized to result in a minimum residual phase error in the OPLL. With this optimal gain $K_{S,opt}$, the phase modulator gain K_P was optimized to result in a minimum phase error in the double-loop and composite PLL configurations. The calculated spectra of the residual phase error in the loop for the different cases are plotted in figure 2.21. The values of the optimum gain and the residual phase error calculated over an integration bandwidth of ±50 MHz are tabulated in table 2.2. It can be seen that the standard deviation of the residual phase error is reduced by a factor of 3–4 due to the addition of phase modulator control.

Note that the calculated loop performance is limited by the assumed values of the propagation delay. The values used in the calculations are an order of magnitude larger than the delays that can be achieved using integrated optoelectronic circuits, and therefore the residual phase error achievable in integrated OPLL circuits is ex-

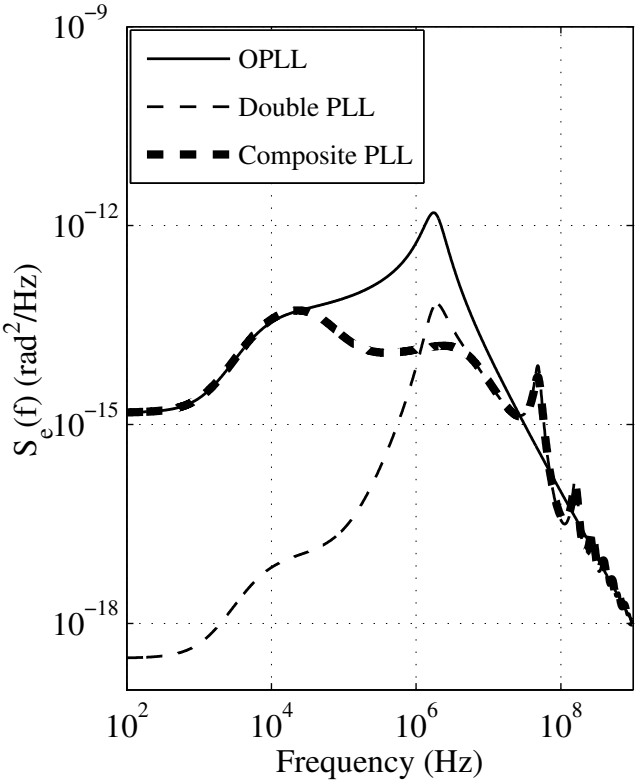

Figure 2.21. Calculated two-sided spectral densities of the residual phase error in the loop, according to equations (2.18), (2.56) and (2.60). The variance of the phase error is the area under the curves. The values of the parameters used in the calculations are listed in the text and in table 2.2.

Table 2.2. Parameters and results of the numerical calculations of the performance of composite OPLLs

System type	Optimal gain	Min. phase error ($\pm$ 50 MHz BW)
Heterodyne OPLL	$K_{S,opt} = 1.4 \times 10^8$ Hz	$\sigma_\phi = 0.43$ rad
Double-loop	$K_{S,opt} = 1.4 \times 10^8$ Hz $K_{P,opt} = 71.5$	$\sigma_\phi = 0.13$ rad
Composite PLL	$K_{S,opt} = 1.4 \times 10^8$ Hz $K_{P,opt} = 65.8$	$\sigma_\phi = 0.12$ rad

pected to be much smaller. For example, in the composite PLL of figure 2.19, if the delays τ_1 and τ_2 are decreased by one order of magnitude to be equal to 0.8 ns, and if the time constants in the filter $F_P(f)$, viz. τ_{Pz} and τ_{Pp2}, are correspondingly reduced by one order of magnitude, a minimum phase error of $\sigma_\phi = 0.039$ rad over a bandwidth of ± 1 GHz is obtained.

2.7.2.3 Experimental Validation

The reduction in residual phase noise was demonstrated using commercial distributed feedback lasers (JDS-Uniphase) in systems with fiber optical and discrete electronic components (MiniCircuits, Brooklyn, NY). A fiber-coupled $LiNbO_3$ optical phase modulator (EOSpace, Redmond, WA) was used in the experiments, and a narrow-linewidth fiber laser (NP Photonics) was used as the master laser. An RF electronic offset frequency of 1.5 GHz was used in the experiments. The error in the loop was calculated using the (heterodyne) beat signal between the master laser and the phase-locked optical output, and integrating the spectrum.

Double-loop configuration. The double-loop configuration shown in figure 2.18 was constructed with optimized loop filters $F_S(f)$ and $F_P(f)$ as given in equations (2.61) and (2.62), with $\tau_{Sz} = 24$ µs, $\tau_{Sp} = 124$ µs, $\tau_{Pz} = 7.5$ ns and $\tau_{Pp1} = 0.66$ µs. The measured beat signals for (a) the OPLL and (b) the combined double-loop system are shown in figure 2.22. A reduction in the residual phase error (± 50 MHz bandwidth) from 0.31 to 0.16 rad was measured.

Composite PLL. A second, similar SCL was used in the construction of the composite PLL shown in figure 2.19. The loop filter parameters of equations (2.61) and (2.62) were chosen to be $\tau_{Sz} = 24$ µs, $\tau_{Sp} = 124$ µs, $\tau_{Pz} = 15$ ns and $\tau_{Pp1} = 1.3$ µs. The measured spectra of the beat signals corresponding to (a) a conventional heterodyne OPLL using this SCL and (b) the composite PLL are shown in figure 2.23. The residual phase error (± 50 MHz bandwidth) is reduced from 0.28 to 0.13 rad.

The experimentally measured reductions in the phase noise for both the above

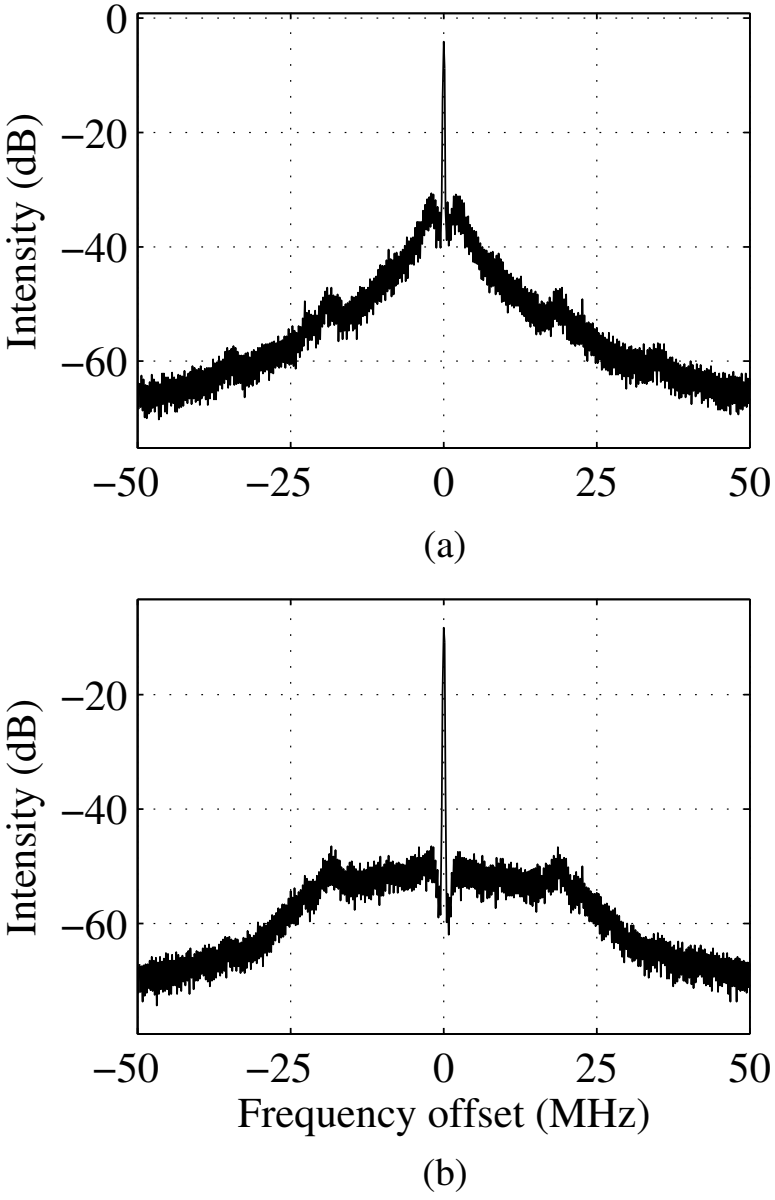

Figure 2.22. Measured spectrum of the beat signal between the optical output and the master laser for an SCL in (a) a heterodyne OPLL, and (b) a double-loop feedback system shown in figure 2.18. Resolution bandwidth = 30 kHz, video bandwidth = 300 Hz.

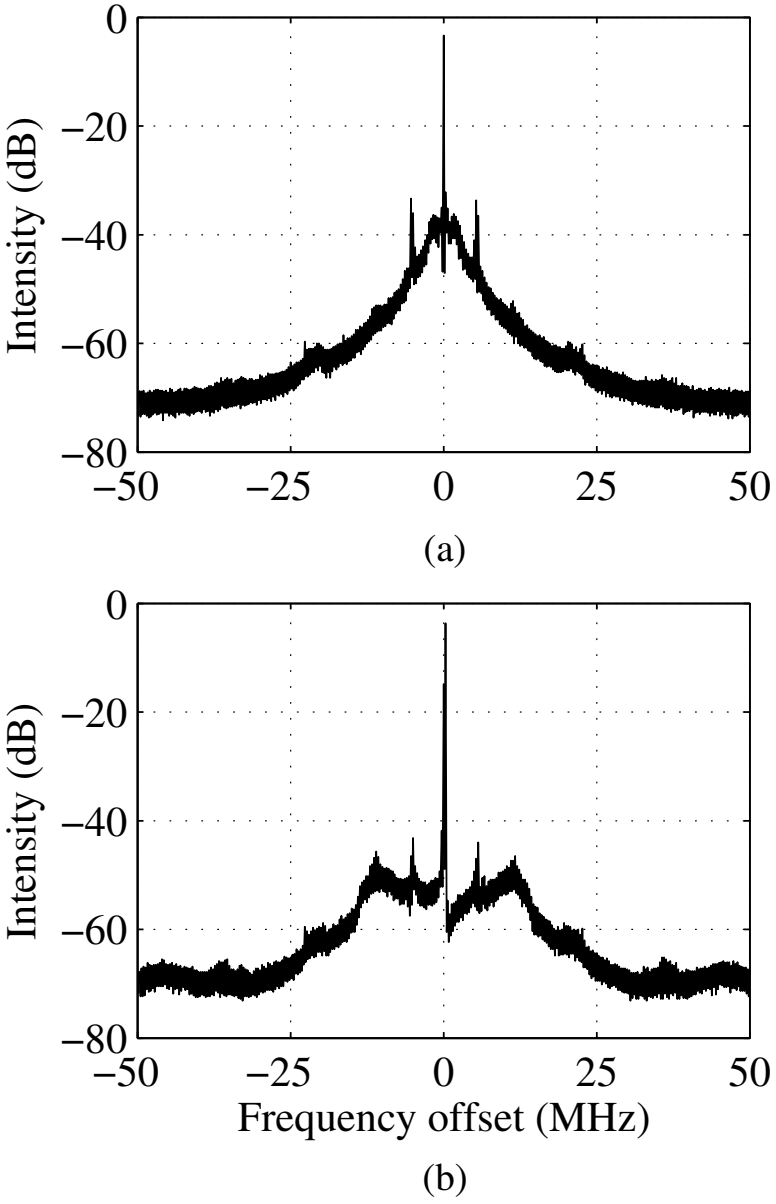

Figure 2.23. Measured spectrum of the beat signal between the optical output and the master laser for an SCL in (a) a heterodyne OPLL, and (b) a composite PLL shown in figure 2.19. Resolution bandwidth = 30 kHz, video bandwidth = 300 Hz.

systems are in fair agreement with the theoretical calculations in table 2.2. The numerical calculations are not exact and are only representative of the expected improvements, since nominal values for the propagation delay and the lineshape of the free-running SCL were assumed. We note that recent independent experiments [38,39] have demonstrated results consistent with figure 2.21 using a feedback system similar to the one developed and analyzed in this work.

2.7.3 Summary

We have proposed and demonstrated experimentally that the residual phase error between the phase-locked optical output of an SCL and the master laser in an OPLL can be further reduced by additional phase correction using an optical phase modulator. *Feedback into the SCL is essential* to compensate for frequency drifts of the SCL due to environmental fluctuations. The use of the additional phase modulator allows large loop bandwidths to be achieved, limited only by propagation delay in the system, as opposed to nonuniformities in the response of the laser. We have demonstrated the phase modulator can be used in two different configurations, both of which yield a considerable reduction in the residual phase error. The experimental demonstrations used fiber optical components and discrete electronic amplifiers and mixers, which caused a large propagation delay and limited the loop bandwidths. The use of integrated photonic circuits in hybrid integrated OPLL systems using these techniques can enable bandwidths of up to a few gigahertz using standard single-section semiconductor lasers and relatively little increase in system complexity.